Commun. Comput. Phys.
doi: 10.4208/cicp.OA-2021-0153

Vol. **31**, No. 3, pp. 669-706
March 2022

Unified Gas-Kinetic Wave-Particle Methods VI: Disperse Dilute Gas-Particle Multiphase Flow

Xiaojian Yang[1], Chang Liu[2], Xing Ji[3], Wei Shyy[1] and Kun Xu[1,3,4,5,*]

[1] *Department of Mechanical and Aerospace Engineering, Hong Kong University of Science and Technology, Clear Water Bay, Kowloon, Hong Kong, China.*
[2] *Institute of Applied Physics and Computational Mathematics, Beijing, China.*
[3] *Department of Mathematics, Hong Kong University of Science and Technology, Clear Water Bay, Kowloon, Hong Kong, China.*
[4] *Guangdong-Hong Kong-Macao Joint Laboratory for Data-Driven Fluid Mechanics and Engineering Applications, Hong Kong University of Science and Technology, Hong Kong, China.*
[5] *Shenzhen Research Institute, Hong Kong University of Science and Technology, Shenzhen, China.*

Received 18 July 2021; Accepted (in revised version) 4 December 2021

Abstract. A coupled gas-kinetic scheme (GKS) and unified gas-kinetic wave-particle (UGKWP) method for the disperse dilute gas-particle multiphase flow is proposed. In the two-phase flow, the gas phase is always in the hydrodynamic regime and is followed by GKS for the Navier-Stokes solution. The particle phase is solved by UGKWP in all regimes from particle trajectory crossing to the hydrodynamic wave interaction with the variation of particle's Knudsen number. In the intensive particle collision regime, the UGKWP gives a hydrodynamic wave representation for the particle phase and the GKS-UGKWP for the two-phase flow reduces to the two-fluid Eulerian-Eulerian (EE) model. In the rarefied regime, the UGKWP tracks individual particle and the GKS-UGKWP goes back to the Eulerian-Lagrangian (EL) formulation. In the transition regime for the solid particle, the GKS-UGKWP takes an optimal choice for the wave and particle decomposition for the solid particle phase and connects the EE and EL methods seamlessly. The GKS-UGKWP method will be tested in all flow regimes with a large variation of Knudsen number for the solid particle transport and Stokes number for the two-phase interaction. It is confirmed that GKS-UGKWP is an efficient and accurate multiscale method for the gas-particle two-phase flow.

AMS subject classifications: 65M08, 76T15, 76P05, 82B40

Key words: Unified gas-kinetic wave-particle method, gas-kinetic scheme, disperse gas-particle two-phase flow.

*Corresponding author. *Email addresses:* xyangbm@connect.ust.hk (X. Yang), liuchang@iapcm.ac.cn (C. Liu), xjiad@connect.ust.hk (X. Ji), weishyy@ust.hk (W. Shyy), makxu@ust.hk (K. Xu)

1 Introduction

Gas-particle flow is a common two-phase system and it appears in both natural phenomena and engineering industries, such as volcanic eruption, sandstorm propagation, chemical transport, and combustion process, etc [3, 11, 18, 40]. Numerical simulations become powerful and indispensable tools for the study of gas-particle system due to the complex physics and difficulties in the experiments and theoretical analysis. Therefore, the development of reliable, accurate, and efficient numerical algorithm to study the multiscale transport associated with different flow regimes is highly demanding in both scientific research and engineering application.

The flow physics of the gas-particle system is very complicated due to particle-particle collision and particle-gas interaction. While the gas phase is in continuum flow regime and modeled by the Navier-Stokes equations, the particle phase can cover a wide range of flow regimes with multiscale transport mechanism [29, 40, 54]. The simulation of gas-particle flow has to include the gas-particle interaction and particle-particle collision. The flow physics is mainly controlled by two non-dimensional parameters, Stokes number St and Knudsen number Kn_s [40]. The Stokes number is related to the drag force on the particle exerted by the surrounding gas flow, which accounts for the momentum exchange between gas and solid particle phase. The dusty flow model is an example in the continuum flow regime when the Stokes number can be very small [46, 49]. Besides, the heat conduction between the gas and solid particle leads to the energy exchange.

Another important parameter is the Knudsen number, characterizing the flow regime of particle phase. At small Knudsen number, the intensive particle-particle collision drives the particle phase to a local equilibrium state and evolves as a continuum flow. Then, the Eulerian-Eulerian (EE) model is usually employed for the gas-particle system under the Eulerian framework, and the EE model is also called two fluid model (TFM). Many studies have been conducted using TFM [2, 22, 46, 50]. The kinetic theory-based granular flow (KTGF) is one representative method of TFM. Based on the analogy between the solid particle behavior in a granular flow and the molecule movement, the kinetic theory is used to get the granular flow equations [8,23,38], which is further extended to the disperse gas-particle system [14, 65]. Since the particle size is large in granular flow, the particle-particle collision should be inelastic, which distinguishes the dynamics of solid particles and molecules [38]. The limitation of TFM is that it cannot describe the non-equilibrium state under the quasi-equilibrium assumption [3]. A representative non-equilibrium phenomenon of disperse phase is the particle trajectory crossing (PTC), which occurs in the extremely dilute flow regime with a large Knudsen number [40]. The TFM fails to capture the PTC transport [16]. The TFM is mostly applicable in the fluid dynamic regime for both gas and particle phase [40].

On the other hand, when the Knudsen number is not very small, the local equilibrium assumption for disperse phase is no longer satisfied. Therefore, both the transport and collision processes have to be considered for the particle phase movement. Under such a non-equilibrium flow regime, the Eulerian-Lagrangian (EL) model is usually adopted.

In the EL model, the governing equations of gas phase are discretized in the Eulerian framework, while the particle is tracked discretely in the Lagrangian formulation. The representative methods of EL model include direct numerical simulation (DNS) [34, 39], computational fluid dynamic-discrete element method (CFD-DEM) [19, 35], multiphase particle-in-cell (MP-PIC) [1, 42, 51, 54], etc. In order to reduce the number of simulating particles, many particles are collected as a particle parcel in the coarse graining particle method (CGPM) [21, 36, 37]. For the EL model, the number of solid particles or parcels used in the simulation is an important factor to determine the computation cost and accuracy. With the increase of particle collision in the near continuum flow regime, the computational cost for tracking particles becomes unaffordable. The hydrodynamic flow solver is preferred in the continuum flow regime. Therefore, great effort has been paid to connect the modeling in different flow regimes. Studies targeting on the multiscale methods have been conducted for the gas-particle system, such as unified gas kinetic scheme (UGKS) [29,55,61], discrete unified gas kinetic scheme (DUGKS) [53], unified gas kinetic particle method (UGKP) [56, 68], method of moment (MOM) [13, 15, 40, 45], direct simulation Monte Carlo (DSMC) [5], hybrid finite-volume-particle method [10], etc.

The UGKS is a discrete velocity method (DVM) for multiscale flow dynamics [61]. The time accumulating evolution solution from particle transport and collision within a time step is used in UGKS for the flux construction under the finite volume framework [60]. The time step in UGKS is not limited by the particle collision time, and it can take a similar value as the conventional NS solver in the continuum flow regime. Besides the neutral gas flow, the UGKS has been successfully applied to many other transport problems, such as radiation and plasma [30, 31, 52, 69]. In particular, an effective multiscale scheme based on the UGKS for the disperse dilute gas-particle system has been proposed [29]. In order to further improve the efficiency of the scheme in the highly rarefied regime, a particle-based UGKS has been developed, which is named unified gas-kinetic particle (UGKP) [33, 68]. The particles in UGKP are categorized as the free transport particle and the collisional particle. The collisional particle within a time step will be eliminated and get re-sampled again from the equilibrium state at the beginning of the next time step. Therefore, only the collisionless particle is fully tracked in UGKP. As a further development, it is realized that the flux from the collisional particle in UGKP can be evaluated analytically. As a result, the collisional particles don't need to be sampled, but represented and evolved with analytical wave in the unified gas-kinetic wave-particle (UGKWP) method [9, 28, 32, 33, 62, 63, 68]. In the continuum flow regime, no particle appears and only wave part survives in UGKWP, which goes back automatically to a hydrodynamic NS flow solver. In the highly rarefied flow regime, the flow evolution will be controlled by the particle transport alone and the UGKWP becomes a particle method. In the transition regime, the UGKWP decomposes the particle distribution function into wave and particle according to the cell's Knudsen number. The UGKWP provides an optimal choice to simulate multiscale transport in different regimes. In this paper, a multiscale method will be developed for the two-phase system, such as the coupled evolution of gas-kinetic scheme (GKS) for the gas phase and the UGKWP

for the particle phase [58, 59]. The GKS is a gas-kinetic theory-based NS solver which is also the limiting scheme of UGKWP in the continuum flow regime [24, 25, 64, 67]. For the continuum flow, the GKS has been successfully used in the turbulence [6, 7], acoustic wave [66], multi-component flow [43, 57], and hypersonic flow studies [27].

The paper is organized as the following. In Section 2, the governing equations for the gas-particle two-phase system are introduced. Section 3 is about the construction of the UGKWP for solid particle phase, GKS for the gas phase, and the coupling between two phases. The numerical experiments are conducted to validate the proposed method in Section 4. Section 5 is the conclusion.

2 Governing equations for gas-particle system

2.1 Governing equations for the particle phase

The evolution of the particle phase is governed by the kinetic equation [4],

$$\frac{\partial f_s}{\partial t}+\nabla_x\cdot(\mathbf{u}f_s)+\nabla_u\cdot(\mathbf{a}f_s+\mathbf{G}f_s)=\frac{g_s-f_s}{\tau_s}, \tag{2.1}$$

where $\mathbf{u}$ is the particle velocity, $\mathbf{a}$ is the particle acceleration caused by the interactive force between particle phase and gas phase, $\mathbf{G}$ is the gravitational acceleration, ∇_x is the divergence operator with respect to space, ∇_u is the divergence operator with respect to velocity, τ_s is the relaxation time for the particle phase, f_s is the distribution function of particle phase, and g_s is the associated equilibrium distribution, which can be written as

$$g_s=\epsilon_s\rho_s\left(\frac{\lambda_s}{\pi}\right)^{\frac{K_s+3}{2}}e^{-\lambda_s\left[(\mathbf{u}-\mathbf{U}_s)^2+\boldsymbol{\xi}^2\right]},$$

where ϵ_s is the volume fraction of particle phase, ρ_s is the material density of particle phase, λ_s is the value relevant to the granular temperature T_s with $\lambda_s=\frac{m_s}{2k_BT_s}$, $m_s=\rho_s\frac{4}{3}\pi\left(\frac{d_s}{2}\right)^3$ is the mass of one particle, d_s is the diameter of the solid particle, and $\mathbf{U}_s$ is the macroscopic velocity of particle phase. K_s is the internal degree of freedom of particle phase, such as the rotational motion, and it is taken 0 in the current study.

For the inelastic collision between particles, the sum of the kinetic and thermal energy for colliding particles may not be conserved. Therefore, the collision term should satisfy the following compatibility condition,

$$\frac{1}{\tau_s}\int g_s\boldsymbol{\psi}\mathrm{d}\Xi=\frac{1}{\tau_s}\int f_s\boldsymbol{\psi}'\mathrm{d}\Xi, \tag{2.2}$$

where $\boldsymbol{\psi}=\left(1,\mathbf{u},\frac{1}{2}\left(\mathbf{u}^2+\boldsymbol{\xi}^2\right)\right)^T$ and $\boldsymbol{\psi}'=\left(1,\mathbf{u},\frac{1}{2}\left(\mathbf{u}^2+\boldsymbol{\xi}^2\right)+\frac{r^2-1}{2}\left(\mathbf{u}-\mathbf{U}_s\right)^2\right)^T$. The lost energy due to inelastic collision in 3D can be written as

$$Q_{loss}=\frac{\left(1-r^2\right)3p_s}{2},$$

where $r \in [0,1]$ is the restitution coefficient for the determination of percentage of lost energy in the inelastic collision. While $r=1$ means no energy loss (elastic collision), $r=0$ refers to total loss of all internal energy of particle phase $\epsilon_s\rho_s e_s = \frac{3}{2}p_s$, where $p_s = \frac{\epsilon_s\rho_s}{2\lambda_s}$.

In order to evaluate the acceleration, the external force of particle phase has to be determined. Here, the drag force $\mathbf{D}$ and the buoyancy force $\mathbf{F}_b$ are considered, which stand for the forces applied on the solid particle by gas phase. The following drag force model is taken,

$$\mathbf{D} = \frac{m_s}{\tau_{st}}\left(\mathbf{U}_g - \mathbf{u}\right), \tag{2.3}$$

where $\mathbf{U}_g$ is the macroscopic velocity of gas phase, and τ_{st} is the particle internal response time, which can be written as

$$\tau_{st} = \frac{4}{3}\frac{\rho_s d_s}{C_d\rho_g|\mathbf{U}_g - \mathbf{u}|}. \tag{2.4}$$

C_d is the drag coefficient, and the Kliatchko model is employed to obtain C_d in this paper [17],

$$C_d = \begin{cases} \dfrac{24}{Re_s} + \dfrac{4}{Re_s^{1/3}}, & Re_s \le 1000, \\ 0.424, & Re_s > 1000, \end{cases} \tag{2.5}$$

where d_s is the diameter of solid particle, and μ_g is the dynamic viscosity of gas phase. $Re_s = |\mathbf{U}_g - \mathbf{u}|d_s/\nu_g$ is the particle Reynolds number, and $\nu_g = \mu_g/\rho_g$ is the kinematic viscosity of gas phase. Besides, another interactive force considered is the buoyancy force, which can be modeled as

$$\mathbf{F}_b = -\frac{m_s}{\rho_s}\nabla_x p_g, \tag{2.6}$$

where p_g is the pressure of gas phase. Therefore, the acceleration of one particle caused by the inter-phase force can be written as

$$\mathbf{a} = \frac{\mathbf{D}+\mathbf{F}_b}{m_s}. \tag{2.7}$$

When the collisions between solid particles are elastic with $r=1$, in the continuum flow regime the hydrodynamic equations become the Euler equations which can be obtained based on the Chapman-Enskog asymptotic analysis given in Appendix A,

$$\begin{aligned}
&\frac{\partial(\epsilon_s\rho_s)}{\partial t} + \nabla_x\cdot(\epsilon_s\rho_s\mathbf{U}_s) = 0, \\
&\frac{\partial(\epsilon_s\rho_s\mathbf{U}_s)}{\partial t} + \nabla_x\cdot(\epsilon_s\rho_s\mathbf{U}_s\mathbf{U}_s + p_s\mathbb{I}) = \frac{\epsilon_s\rho_s\left(\mathbf{U}_g - \mathbf{U}_s\right)}{\tau_{st}} - \epsilon_s\nabla_x p_g + \epsilon_s\rho_s\mathbf{G}, \\
&\frac{\partial(\epsilon_s\rho_s E_s)}{\partial t} + \nabla_x\cdot((\epsilon_s\rho_s E_s + p_s)\mathbf{U}_s) = \frac{\epsilon_s\rho_s\mathbf{U}_s\cdot\left(\mathbf{U}_g - \mathbf{U}_s\right)}{\tau_{st}} - \epsilon_s\mathbf{U}_s\cdot\nabla_x p_g + \epsilon_s\rho_s\mathbf{U}_s\cdot\mathbf{G} - \frac{3p_s}{\tau_{st}}.
\end{aligned} \tag{2.8}$$

When the collision is inelastic with $r=0$, the governing equations would be the pressureless Euler equations.

Besides, the heat conduction between the particle and gas phase will be considered, which is associated with the temperature change. For particle phase, the material temperature of particle phase is denoted as T_s^m, which is different from the granular temperature T_s. The governing equation for T_s^m in 3D can be written as [22]

$$\frac{\partial(\epsilon_s\rho_s C_s T_s^m)}{\partial t}+\nabla_x\cdot(\epsilon_s\rho_s C_s T_s^m\mathbf{U}_s)=\epsilon_s\rho_s C_s\frac{T_g-T_s^m}{\tau_T}+\frac{Q_{loss}}{\tau_s}, \tag{2.9}$$

where C_s is the specific heat capacity of the particle phase. $\tau_T=\frac{\rho_s C_s r_s}{3h}$ is the relaxation time for heat conduction, where $r_s=d_s/2$ is the radius of the solid particle and h is the convection coefficient between solid material and gas phase. The first term on right hand side stands for the heat conduction between particle phase and gas phase, while the second term on the right hand side is the lost energy due to the inelastic collision between solid particles. Here we assume that all the lost energy in inelastic collision is transferred into the internal energy of the solid particles.

In summary, the evolution of particle phase is governed by Eq. (2.1) and Eq. (2.9).

2.2 Governing equations for the gas phase

The gas phase is regarded as the continuum flow and the macroscopic governing equations are the Navier-Stokes (NS) equations with the source terms to account for the gas-particle interaction,

$$\begin{aligned}
&\frac{\partial(\widetilde{\rho_g})}{\partial t}+\nabla_x\cdot(\widetilde{\rho_g}\mathbf{U}_g)=0,\\
&\frac{\partial(\widetilde{\rho_g}\mathbf{U}_g)}{\partial t}+\nabla_x\cdot(\widetilde{\rho_g}\mathbf{U}_g\mathbf{U}_g+\widetilde{p_g}\mathbb{I}-\widetilde{\mu_g}\boldsymbol{\sigma})=-\frac{\epsilon_s\rho_s(\mathbf{U}_g-\mathbf{U}_s)}{\tau_{st}}+\epsilon_s\nabla_x p_g,\\
&\frac{\partial(\widetilde{\rho_g}E_g)}{\partial t}+\nabla_x\cdot\left((\widetilde{\rho_g}E_g+\widetilde{p_g})\mathbf{U}_g-\widetilde{\mu_g}\boldsymbol{\sigma}\cdot\mathbf{U}_g+\widetilde{\kappa}\nabla_x T_g\right)=-\frac{\epsilon_s\rho_s\mathbf{U}_s\cdot(\mathbf{U}_g-\mathbf{U}_s)}{\tau_{st}}+\epsilon_s\mathbf{U}_s\cdot\nabla_x p_g\\
&\qquad\qquad+\frac{3p_s}{\tau_{st}}-\epsilon_s\rho_s C_s\frac{T_g-T_s^m}{\tau_T},
\end{aligned} \tag{2.10}$$

where $p_g=\rho_g RT_g$ is the pressure of gas phase and $\widetilde{p_g}=\widetilde{\rho_g}RT_g$, the strain rate tensor $\boldsymbol{\sigma}$ is given by

$$\boldsymbol{\sigma}=\nabla_x\mathbf{U}_g+(\nabla_x\mathbf{U}_g)^T-\frac{2}{3}\nabla_x\cdot\mathbf{U}_g\mathbb{I},$$

and

$$\widetilde{\mu_g}=\tau_g\widetilde{p_g},\quad \widetilde{\kappa}=\frac{5}{2}R\tau_g\widetilde{p_g}.$$

3 Numerical scheme for gas-particle system

3.1 UGKWP for the particle phase

In this subsection, the evolution of the particle phase by UGKWP method is introduced. Generally, the particle phase kinetic equation Eq. (2.1) is split as

$$\mathcal{L}_{s1}: \ \frac{\partial f_s}{\partial t}+\nabla_x\cdot(\mathbf{u}f_s)=\frac{g_s-f_s}{\tau_s}, \tag{3.1}$$

$$\mathcal{L}_{s2}: \ \frac{\partial f_s}{\partial t}+\nabla_u\cdot(\mathbf{a}f_s+\mathbf{G}f_s)=0. \tag{3.2}$$

Firstly, we focus on $\mathcal{L}_{s1}$ part. Consider the kinetic equation for particle phase without external force,

$$\frac{\partial f_s}{\partial t}+\nabla_x\cdot(\mathbf{u}f_s)=\frac{g_s-f_s}{\tau_s}.$$

For brevity, the subscript s standing for the solid particle phase will be neglected in this subsection. The integration solution of the kinetic equation can be written as

$$f(\mathbf{x},t,\mathbf{u},\boldsymbol{\xi})=\frac{1}{\tau}\int_0^t g(\mathbf{x}',t',\mathbf{u},\boldsymbol{\xi})e^{-(t-t')/\tau}\mathrm{d}t'+e^{-t/\tau}f_0(\mathbf{x}-\mathbf{u}t,\mathbf{u},\boldsymbol{\xi}), \tag{3.3}$$

where $\mathbf{x}'=\mathbf{x}+\mathbf{u}(t'-t)$ is the particle trajectory, f_0 is the initial gas distribution function at time $t=0$, and g is the corresponding equilibrium state.

In UGKWP, both the macroscopic variables and the gas distribution function need to be updated. Generally, in the finite volume framework, the cell-averaged macroscopic variables $\mathbf{W}_i$ of cell i can be updated by the following equation,

$$\mathbf{W}_i^{n+1}=\mathbf{W}_i^n-\frac{1}{\Omega_i}\sum_{S_{ij}\in\partial\Omega_i}\mathbf{F}_{ij}S_{ij}, \tag{3.4}$$

where $\mathbf{W}_i=(\rho_i,\rho_i\mathbf{U}_i,\rho_iE_i)$ are the cell-averaged macroscopic variables,

$$\mathbf{W}_i=\frac{1}{\Omega_i}\int_{\Omega_i}\mathbf{W}(\mathbf{x})\,\mathrm{d}\Omega,$$

Ω_i is the volume of cell i, $\partial\Omega_i$ denotes the set of interface of cell i, S_{ij} is one interface of cell i, $\mathbf{F}_{ij}$ denotes the macroscopic flux across the interface S_{ij}, which can be written as

$$\mathbf{F}_{ij}=\int_0^{\Delta t}\int\mathbf{u}\cdot\mathbf{n}_{ij}f_{ij}(\mathbf{x},t,\mathbf{u},\boldsymbol{\xi})\boldsymbol{\psi}\mathrm{d}\Xi\mathrm{d}t, \tag{3.5}$$

where $\mathbf{n}_{ij}$ denotes the normal vector of interface S_{ij}, $f_{ij}(t)$ is the time-dependent distribution function on the interface S_{ij}, $\boldsymbol{\psi}=(1,\mathbf{u},\frac{1}{2}(\mathbf{u}^2+\boldsymbol{\xi}^2))^T$, and $\mathrm{d}\Xi=\mathrm{d}\mathbf{u}\mathrm{d}\boldsymbol{\xi}$.

Substituting the time-dependent distribution function Eq. (3.3) into Eq. (3.5), the flux can be obtained,

$$\begin{aligned}\mathbf{F}_{ij} &= \int_0^{\Delta t}\int \mathbf{u}\cdot\mathbf{n}_{ij} f_{ij}(\mathbf{x},t,\mathbf{u},\boldsymbol{\xi})\boldsymbol{\psi}\mathrm{d}\Xi\mathrm{d}t \\ &= \int_0^{\Delta t}\int \mathbf{u}\cdot\mathbf{n}_{ij}\left[\frac{1}{\tau}\int_0^t g(\mathbf{x}',t',\mathbf{u},\boldsymbol{\xi})e^{-(t-t')/\tau}\mathrm{d}t'\right]\boldsymbol{\psi}\mathrm{d}\Xi\mathrm{d}t \\ &\quad + \int_0^{\Delta t}\int \mathbf{u}\cdot\mathbf{n}_{ij}\left[e^{-t/\tau}f_0(\mathbf{x}-\mathbf{u}t),\mathbf{u},\boldsymbol{\xi}\right]\boldsymbol{\psi}\mathrm{d}\Xi\mathrm{d}t \\ &\overset{def}{=} \mathbf{F}_{ij}^{eq}+\mathbf{F}_{ij}^{fr}.\end{aligned}$$

The procedure of obtaining the local equilibrium state g_0 at the cell interface as well as the construction of $g(t)$ is the same as that in GKS [59]. For second order accuracy, the equilibrium state g around the cell interface is written as

$$g\left(\mathbf{x}',t',\mathbf{u},\boldsymbol{\xi}\right)=g_0(\mathbf{x},\mathbf{u},\boldsymbol{\xi})\left(1+\overline{\mathbf{a}}\cdot\mathbf{u}\left(t'-t\right)+\bar{A}t'\right),$$

where $\overline{\mathbf{a}}=[\overline{a_1},\overline{a_2},\overline{a_3}]^T$, $\overline{a_i}=\frac{\partial g}{\partial x_i}/g$, $i=1,2,3$, $\overline{A}=\frac{\partial g}{\partial t}/g$, and g_0 is the local equilibrium state on the interface. More specifically, the coefficients of spatial derivatives $\overline{a_i}$ can be obtained from the associated derivatives of macroscopic variables,

$$\langle\overline{a_i}\rangle=\partial\mathbf{W}_0/\partial x_i,$$

where $i=1,2,3$, and $\langle\cdots\rangle$ means the moments of the Maxwellian distribution functions,

$$\langle\cdots\rangle=\int\boldsymbol{\psi}(\cdots)g\mathrm{d}\Xi.$$

The coefficients of temporal derivative $\overline{A}$ in 3D can be determined by the compatibility condition,

$$\left\langle\overline{\mathbf{a}}\cdot\mathbf{u}+\overline{A}\right\rangle=\begin{bmatrix}0\\ \mathbf{0}\\ -\frac{Q_{loss}}{\tau_s}\end{bmatrix},$$

where $Q_{loss}=\frac{(1-r^2)3p_s}{2}$, and the last term is caused by the lost energy due to the particle-particle inelastic collision.

With the determination of all coefficients in $g(\mathbf{x}',t',\mathbf{u},\boldsymbol{\xi})$ for the equilibrium state, its integration becomes

$$\begin{aligned}f^{eq}(\mathbf{x},t,\mathbf{u},\boldsymbol{\xi}) &\overset{def}{=} \frac{1}{\tau}\int_0^t g(\mathbf{x}',t',\mathbf{u},\boldsymbol{\xi})e^{-(t-t')/\tau}\mathrm{d}t' \\ &= c_1 g_0(\mathbf{x},\mathbf{u},\boldsymbol{\xi})+c_2\overline{\mathbf{a}}\cdot\mathbf{u}g_0(\mathbf{x},\mathbf{u},\boldsymbol{\xi})+c_3 A g_0(\mathbf{x},\mathbf{u},\boldsymbol{\xi}),\end{aligned}\tag{3.6}$$

with coefficients,

$$\begin{aligned} c_1 &= 1-e^{-t/\tau}, \\ c_2 &= (t+\tau)e^{-t/\tau}-\tau, \\ c_3 &= t-\tau+\tau e^{-t/\tau}, \end{aligned}$$

and thereby the total flux transport over a time step for equilibrium state can be obtained,

$$\mathbf{F}_{ij}^{eq} = \int_0^{\Delta t} \int \mathbf{u}\cdot\mathbf{n}_{ij} f_{ij}^{eq}(\mathbf{x},t,\mathbf{u},\boldsymbol{\xi})\boldsymbol{\psi} \mathrm{d}\Xi \mathrm{d}t.$$

Besides, the flux contributed by the free transport of f_0 is calculated by tracking the particles sampled from f_0. Therefore, the updating of the cell-averaged macroscopic variables can be written as

$$\mathbf{W}_i^{n+1} = \mathbf{W}_i^n - \frac{1}{\Omega_i}\sum_{S_{ij}\in\partial\Omega_i} \mathbf{F}_{ij}^{eq} S_{ij} + \frac{\mathbf{w}_i^{fr}}{\Omega_i} + \Delta t \mathbf{S}_i, \tag{3.7}$$

where $\mathbf{w}_i^{fr}$ is the net free streaming flow of cell i, standing for the flux contribution of the free streaming of particles, and the term $\mathbf{S}_i = \left[0,\mathbf{0},-\frac{Q_{loss}}{\tau_s}\right]^T$ is the source term in 3D due to the inelastic collision for solid particle phase.

Now it is about how to obtain the net free streaming flow $\mathbf{w}_i^{fr}$. The evolution of particle should also satisfy the integral solution of the kinetic equation, which can be written as

$$f(\mathbf{x},t,\mathbf{u},\boldsymbol{\xi}) = \left(1-e^{-t/\tau}\right) g^+(\mathbf{x},t,\mathbf{u},\boldsymbol{\xi}) + e^{-t/\tau} f_0(\mathbf{x}-\mathbf{u}t,\mathbf{u},\boldsymbol{\xi}), \tag{3.8}$$

where g^+ is named as the hydrodynamic distribution function with analytical formulation. The initial distribution function f_0 has a probability of $e^{-t/\tau}$ to free transport and $(1-e^{-t/\tau})$ to collide with other particles. The post-collision particle satisfies the distribution $g^+(\mathbf{x},\mathbf{u},t)$. The free transport time before the first collision with other particles is called t_c. The cumulative distribution function of t_c is

$$F(t_c<t) = 1-e^{-t/\tau}, \tag{3.9}$$

and therefore t_c can be sampled as $t_c = -\tau\ln(\eta)$, where η is a random number generated from a uniform distribution $U(0,1)$. Then, the free streaming time t_f for particle k is determined by

$$t_f = \min[-\tau\ln(\eta),\Delta t], \tag{3.10}$$

where Δt is the time step. Therefore, in one time step, all particles can be divided into two groups: the collisionless particles and the collisional particles, which are determined by the relation between of the time step Δt and free streaming time t_f. Specifically, if

$t_f = \Delta t$ for a particle, it is the collisionless particle, and the trajectory of this particle is fully tracked in the whole time step. On the contrary, if $t_f < \Delta t$ for a particle, it is the collisional particle and its trajectory will be tracked until t_f. Subsequently, this particle is eliminated in the simulation, and the mass, momentum and energy of this particle are merged into the macroscopic quantities of the relevant cell. The particle trajectory in the free streaming process within the time t_f is tracked by

$$\mathbf{x} = \mathbf{x}^n + \mathbf{u}^n t_f. \tag{3.11}$$

The term $\mathbf{w}_i^{fr}$ can be calculated by counting the particles passing through the interfaces of cell i,

$$\mathbf{w}_i^{fr} = \sum_{k \in P\left(\partial\Omega_i^+\right)} \boldsymbol{\phi}_k - \sum_{k \in P\left(\partial\Omega_i^-\right)} \boldsymbol{\phi}_k, \tag{3.12}$$

where $P\left(\partial\Omega_i^+\right)$ is the particle set moving into the cell i during one time step, $P\left(\partial\Omega_i^-\right)$ is the particle set moving out of the cell i during one time step, k is the particle index in one specific set, and $\boldsymbol{\phi}_k = \left[m_k, m_k\mathbf{u}_k, \frac{1}{2}m_k(\mathbf{u}_k^2 + e_k)\right]^T$ is the mass, momentum and energy carried by particle k. Therefore, $\mathbf{w}_i^{fr}/\Omega_i$ is the net conservative variable change caused by the free streaming of all tracked particles. Now, all the terms in Eq. (3.7) have been determined and the macroscopic variables $\mathbf{W}_i$ can be updated.

The trajectories of all particles have been tracked during the time interval $\left(0, t_f\right)$. For the collisionless particles $t_f = \Delta t$, they still survive at the end of one time step; while the collisional particles $t_f < \Delta t$ are deleted after their first collision with other particles and the overall effect from collisional particles is taken into account in the updated conservative flow variables. Therefore, the macroscopic variables of the collisional particles in cell i at the end of each time step can be directly obtained based on the conservation law,

$$\mathbf{W}_i^h = \mathbf{W}_i^{n+1} - \mathbf{W}_i^p, \tag{3.13}$$

where $\mathbf{W}_i^p$ are the total conservative variables from remaining collisionless particles at the end of one time step. Besides, the macroscopic variables $\mathbf{W}_i^h$ is coming from eliminated collisional particles, which can be recovered by re-sampling the collisional particles according to $\mathbf{W}_i^h$ based on a Maxwellian distribution. Now the update of both macroscopic variables as well as the microscopic particles have been finished. The above method is so-called unified gas-kinetic particle (UGKP) method.

The UGKWP method is a further development of UGKP. In UGKP method, all particles can be divided into two types: the collisionless particles, survived at the end of one time step; and collisional particles, deleted after the first collision and re-sampled at the end of one time step. To further improve the efficiency, only the collisionless particles, which will survive in the next whole time step, need to be sampled from $\mathbf{W}_i^h$. The collisional particles from $\mathbf{W}_i^h$ in the next time step can be represented as hydrodynamic wave

with analytical solution. More specifically, in the next time step the transport flux from these un-sampled collisional particles can be evaluated analytically. According to the cumulative distribution in Eq. (3.9), the proportion of the collisionless particles is $e^{-\Delta t/\tau}$, and therefore in UGKWP the portion of macroscopic variables $\mathbf{W}_i^h$ required for sampling collisionless particles in cell i is

$$\mathbf{W}_i^{hp} = e^{-\Delta t/\tau}\mathbf{W}_i^h. \tag{3.14}$$

Note that, the free transport time of all these sampled particles is $t_f = \Delta t$ in UGKWP. Now, the net flow determined by the free streaming of particles are denoted as $\mathbf{w}_i^{fr,p}$, which can be calculated with the same way,

$$\mathbf{w}_i^{fr,p} = \sum_{k\in P\left(\partial\Omega_i^+\right)} \boldsymbol{\phi}_k - \sum_{k\in P\left(\partial\Omega_i^-\right)} \boldsymbol{\phi}_k. \tag{3.15}$$

Besides, the free transport flux from these un-sampled collisional particles from $(1-e^{-\Delta t/\tau})\mathbf{W}_i^h$ are evaluated as

$$\begin{aligned}
\mathbf{F}_{ij}^{fr,wave} &= \mathbf{F}_{ij}^{fr,UGKS}(\mathbf{W}_i^h) - \mathbf{F}_{ij}^{fr,DVM}(\mathbf{W}_i^{hp}) \\
&= \int_0^{\Delta t}\int \mathbf{u}\cdot\mathbf{n}_{ij}\left[e^{-t/\tau}f_0(\mathbf{x}-\mathbf{u}t,\mathbf{u},\boldsymbol{\xi})\right]\boldsymbol{\psi}\mathrm{d}\Xi\mathrm{d}t \\
&\quad - e^{-\Delta t/\tau}\int_0^{\Delta t}\int \mathbf{u}\cdot\mathbf{n}_{ij}\left[g_0^h(\mathbf{x},\mathbf{u},\boldsymbol{\xi}) - t\mathbf{u}\cdot g_{\mathbf{x}}^h(\mathbf{x},\mathbf{u},\boldsymbol{\xi})\right]\boldsymbol{\psi}\mathrm{d}\Xi\mathrm{d}t \\
&= \int \mathbf{u}\cdot\mathbf{n}_{ij}\left[\left(q_4 - \Delta t e^{-\Delta t/\tau}\right)g_0^h(\mathbf{x},\mathbf{u},\boldsymbol{\xi}) + \left(q_5 + \frac{\Delta t^2}{2}e^{-\Delta t/\tau}\right)\mathbf{u}\cdot g_{\mathbf{x}}^h(\mathbf{x},\mathbf{u},\boldsymbol{\xi})\right]\boldsymbol{\psi}\mathrm{d}\Xi,
\end{aligned}$$

with the coefficients,

$$\begin{aligned}
q_4 &= \tau\left(1-e^{-\Delta t/\tau}\right), \\
q_5 &= \tau\Delta t e^{-\Delta t/\tau} - \tau^2\left(1-e^{-\Delta t/\tau}\right).
\end{aligned}$$

Then, the macroscopic flow variables in UGKWP can be updated,

$$\mathbf{W}_i^{n+1} = \mathbf{W}_i^n - \frac{1}{\Omega_i}\sum_{S_{ij}\in\partial\Omega_i}\mathbf{F}_{ij}^{eq}S_{ij} - \frac{1}{\Omega_i}\sum_{S_{ij}\in\partial\Omega_i}\mathbf{F}_{ij}^{fr,wave}S_{ij} + \frac{\mathbf{w}_i^{fr,p}}{\Omega_i} + \Delta t\mathbf{S}_i. \tag{3.16}$$

The second part is to evaluate the evolution due to acceleration term in Eq. (3.2),

$$\frac{\partial f_s}{\partial t} + \nabla_u\cdot(\mathbf{a}f_s + \mathbf{G}f_s) = 0,$$

where velocity-dependent acceleration term caused by the inter-phase forces has the following form,

$$\mathbf{a}=\frac{\mathbf{D}+\mathbf{F}_b}{m_s}=\frac{\mathbf{U}_g-\mathbf{u}}{\tau_{st}}-\frac{1}{\rho_s}\nabla_x p_g.$$

Taking moment with $\boldsymbol{\psi}=\left(1,\mathbf{u},\frac{\mathbf{u}^2+\boldsymbol{\xi}^2}{2}\right)^T$ to Eq. (3.2),

$$\int\boldsymbol{\psi}\left(\frac{\partial f_s}{\partial t}+\mathbf{a}\cdot\nabla_u f_s+f_s\nabla_u\cdot\mathbf{a}+\mathbf{G}\cdot\nabla_u f_s+f_s\nabla_u\cdot\mathbf{G}\right)\mathrm{d}\Xi=0,$$

and in the Euler regime $f_s=g_s+\mathcal{O}(\tau_s)$, we can obtain,

$$\frac{\partial\mathbf{W}_s}{\partial t}+(\mathbf{Q}+\mathbf{Q}_G)=0,$$

where

$$\mathbf{W}_s=\begin{bmatrix}\epsilon_s\rho_s\\ \epsilon_s\rho_s\mathbf{U}_s\\ \epsilon_s\rho_s E_s\end{bmatrix},\quad \mathbf{Q}=\begin{bmatrix}0\\ \frac{\epsilon_s\rho_s(\mathbf{U}_s-\mathbf{U}_g)}{\tau_{st}}+\epsilon_s\nabla_x p_g\\ \frac{\epsilon_s\rho_s\mathbf{U}_s\cdot(\mathbf{U}_s-\mathbf{U}_g)}{\tau_{st}}+3\frac{p_s}{\tau_{st}}+\epsilon_s\mathbf{U}_s\cdot\nabla_x p_g\end{bmatrix},\quad \mathbf{Q}_G=\begin{bmatrix}0\\ -\epsilon_s\rho_s\mathbf{G}\\ -\epsilon_s\rho_s\mathbf{U}_s\cdot\mathbf{G}\end{bmatrix}.$$

When the first order forward Euler method is employed for time marching, the cell-averaged macroscopic variables for three-dimensional problems can be updated by

$$\mathbf{W}_s^{n+1}=\mathbf{W}_s-(\mathbf{Q}+\mathbf{Q}_G)\Delta t, \tag{3.17}$$

and the modifications on velocity and location of the remaining free streaming particles are

$$\mathbf{u}^{n+1}=\mathbf{u}+(\mathbf{a}+\mathbf{G})t_f, \tag{3.18}$$

$$\mathbf{x}^{n+1}=\mathbf{x}+\frac{(\mathbf{a}+\mathbf{G})}{2}t_f^2. \tag{3.19}$$

Finally, the evolution of the material temperature T_s^m of the solid phase is calculated. Two factors need to be considered. The first one is the effect of the heat conduction between the particle phase and the gas phase. The exchanged energy rate q_{cond} due to the heat conduction can be evaluated as

$$q_{cond}=\epsilon_s\rho_s C_s\frac{T_g-T_s^m}{\tau_T}.$$

The second factor is the lost energy due to the inelastic collision for the particle phase, which is

$$q_{loss}=\frac{Q_{loss}}{\tau_s}=\frac{(1-r^2)3p_s}{2\tau_s},$$

where $r \in [0,1]$ is the restitution coefficient. With the determination of q_{cond} and q_{loss}, Eq. (2.9) can be used for the evolution of material temperature of solid particles T_s^m,

$$\frac{\partial(\epsilon_s\rho_s C_s T_s^m)}{\partial t}+\nabla_x\cdot(\epsilon_s\rho_s C_s T_s^m \mathbf{U}_s)=\epsilon_s\rho_s C_s\frac{T_g-T_s^m}{\tau_T}+\frac{(1-r^2)3p_s}{2\tau_s}.$$

In this paper, the Lax-Friedrichs method is employed to solve the above equation for the update of material temperature T_s^m in the finite volume framework. Now the complete updating procedure for particle phase in one time step is presented.

3.2 GKS for the gas phase

The gas phase is governed by the Navier-Stokes equations and the corresponding scheme is the gas-kinetic scheme (GKS), which is the limiting scheme of UGKWP in the continuum flow regime without collisionless particles. In general, the gas phase governing equations can be split into three parts,

$$\mathcal{L}_{g1}:\ \begin{cases}\frac{\partial(\widetilde{\rho}_g)}{\partial t}+\nabla_x\cdot(\widetilde{\rho}_g\mathbf{U}_g)=0,\\ \frac{\partial(\widetilde{\rho}_g\mathbf{U}_g)}{\partial t}+\nabla_x\cdot(\widetilde{\rho}_g\mathbf{U}_g\mathbf{U}_g+\widetilde{p}_g\mathbb{I}-\widetilde{\mu}_g\boldsymbol{\sigma})=0,\\ \frac{\partial(\widetilde{\rho}_g E_g)}{\partial t}+\nabla_x\cdot\left((\widetilde{\rho}_g E_g+\widetilde{p}_g)\mathbf{U}_g-\widetilde{\mu}_g\boldsymbol{\sigma}\cdot\mathbf{U}_g+\widetilde{\kappa}\nabla_x T_g\right)=0,\end{cases} \tag{3.20}$$

$$\mathcal{L}_{g2}:\ \begin{cases}\frac{\partial(\widetilde{\rho}_g)}{\partial t}=0,\\ \frac{\partial(\widetilde{\rho}_g\mathbf{U}_g)}{\partial t}=-\frac{\epsilon_s\rho_s(\mathbf{U}_g-\mathbf{U}_s)}{\tau_{st}}+\epsilon_s\nabla_x p_g,\\ \frac{\partial(\widetilde{\rho}_g E_g)}{\partial t}=-\frac{\epsilon_s\rho_s\mathbf{U}_s\cdot(\mathbf{U}_g-\mathbf{U}_s)}{\tau_{st}}+\frac{3p_s}{\tau_{st}}+\epsilon_s\mathbf{U}_s\cdot\nabla_x p_g,\end{cases} \tag{3.21}$$

$$\mathcal{L}_{g3}:\ \frac{\mathrm{d}(\widetilde{\rho}_g C_g T_g)}{\mathrm{d}t}=-\epsilon_s\rho_s C_s\frac{T_g-T_s^m}{\tau_T}, \tag{3.22}$$

where C_g is the specific heat capacity of the gas phase.

Firstly, $\mathcal{L}_{g1}$ is solved by GKS, which is a NS solver based on the kinetic equation. The kinetic equation for the gas phase can be written as

$$\frac{\partial f_g}{\partial t}+\nabla_x\cdot(\mathbf{u}f_g)=\frac{g_g-f_g}{\tau_g}, \tag{3.23}$$

where $\mathbf{u}$ is the particle velocity, τ_g is the relaxation time for gas phase, f_g is the distribution function of gas phase, and g_g is the corresponding equilibrium state (Maxwellian distribution). In the current work, the gravitational acceleration for the gas phase $\mathbf{G}$ is neglected.

The local equilibrium state g_g can be written as

$$g_g=\widetilde{\rho_g}\left(\frac{\lambda_g}{\pi}\right)^{\frac{K+3}{2}}e^{-\lambda_g\left[(\mathbf{u}-\mathbf{U}_g)^2+\boldsymbol{\xi}^2\right]},$$

where $\widetilde{\rho_g}=\epsilon_g\rho_g$ is the apparent density of gas phase, ϵ_g is the volume fraction of particle phase satisfying the relation $\epsilon_s+\epsilon_g=1$, and ρ_g is the density of gas phase. λ_g is determined by gas temperature through $\lambda_g=\frac{m_g}{2k_BT_g}$, where m_g is the molecular mass, $\mathbf{U}_g$ is the averaged macroscopic velocity of gas phase. K is the internal degree of freedom with $K=\frac{5-3\gamma}{\gamma-1}$ for gas phase in 3D, and γ is the specific heat ratio with a value 1.4 for diatomic gas.

The collision term satisfies the compatibility condition

$$\int\frac{g_g-f_g}{\tau_g}\boldsymbol{\psi}\mathrm{d}\Xi=0, \tag{3.24}$$

where $\boldsymbol{\psi}=\left(1,\mathbf{u},\frac{1}{2}(\mathbf{u}^2+\boldsymbol{\xi}^2)\right)^T$, the internal variables $\boldsymbol{\xi}^2=\xi_1^2+\cdots+\xi_K^2$, $\mathrm{d}\Xi=\mathrm{d}\mathbf{u}\mathrm{d}\boldsymbol{\xi}$. In the continuum flow regime, the Navier-Stokes equations (3.20) can be recovered from the above kinetic equation based on the Chapman-Enskog asymptotic analysis, which is shown in the Appendix A of [58].

For brevity, the subscript g standing for the gas phase will be neglected in this subsection. Based on Eq. (3.23), the solution of f at a cell interface can be written as

$$f(\mathbf{x},t,\mathbf{u},\boldsymbol{\xi})=\frac{1}{\tau}\int_0^t g(\mathbf{x}',t',\mathbf{u},\boldsymbol{\xi})e^{-(t-t')/\tau}\mathrm{d}t'+e^{-t/\tau}f_0(\mathbf{x}-\mathbf{u}t,\mathbf{u},\boldsymbol{\xi}), \tag{3.25}$$

where $\mathbf{x}'=\mathbf{x}+\mathbf{u}(t'-t)$ is the particle trajectory, f_0 is the initial gas distribution function at time $t=0$, and g is the corresponding equilibrium state. The initial gas distribution function f_0 can be constructed as

$$f_0=f_0^l(\mathbf{x},\mathbf{u})H(x)+f_0^r(\mathbf{x},\mathbf{u})(1-H(x)), \tag{3.26}$$

where $H(x)$ is the Heaviside function, f_0^l and f_0^r are the initial gas distribution functions on the left and right sides of one cell interface, which can be determined by the corresponding macroscopic variables. The initial gas distribution functions f_0^k, $k=l,r$, are constructed as

$$f_0^k=g^k\left(1+\mathbf{a}^k\cdot\mathbf{x}-\tau(\mathbf{a}^k\cdot\mathbf{u}+A^k)\right),$$

where g^l and g^r are the Maxwellian distribution functions on the left and right hand sides of the cell interface, which are determined by the corresponding conservative variables $\mathbf{W}^l$ and $\mathbf{W}^r$. The coefficients $\mathbf{a}^l=\left[a_1^l,a_2^l,a_3^l\right]^T$, $\mathbf{a}^r=\left[a_1^r,a_2^r,a_3^r\right]^T$ are related to the spatial derivatives in normal and tangential directions, which are obtained from the derivatives of initial macroscopic flow variables,

$$\left\langle a_i^l\right\rangle=\partial\mathbf{W}^l/\partial x_i,\quad\left\langle a_i^r\right\rangle=\partial\mathbf{W}^r/\partial x_i,$$

where $i=1,2,3$, and $\langle\cdots\rangle$ means the moments of the Maxwellian distribution functions,

$$\langle\cdots\rangle=\int\boldsymbol{\psi}(\cdots)g\mathrm{d}\Xi.$$

Based on the Chapman-Enskog expansion, the non-equilibrium part of the distribution function satisfies

$$\left\langle\mathbf{a}^l\cdot\mathbf{u}+A^l\right\rangle=0,\quad\langle\mathbf{a}^r\cdot\mathbf{u}+A^r\rangle=0,$$

from which the coefficients A^l and A^r are fully determined. The equilibrium state g around the cell interface is modeled as

$$g=g_0(1+\overline{\mathbf{a}}\cdot\mathbf{x}+\bar{A}t),\tag{3.27}$$

where $\overline{\mathbf{a}}=[\overline{a}_1,\overline{a}_2,\overline{a}_3]^T$. g_0 is the local equilibrium state at the cell interface. More specifically, g can be determined by the compatibility condition,

$$\begin{aligned}&\int\boldsymbol{\psi}g_0\mathrm{d}\Xi=\mathbf{W}_0=\int_{u>0}\boldsymbol{\psi}g^l\mathrm{d}\Xi+\int_{u<0}\boldsymbol{\psi}g^r\mathrm{d}\Xi,\\&\int\boldsymbol{\psi}\overline{a}_ig_0\mathrm{d}\Xi=\partial\mathbf{W}_0/\partial x_i=\int_{u>0}\boldsymbol{\psi}a_i^lg^l\mathrm{d}\Xi+\int_{u<0}\boldsymbol{\psi}a_i^rg^r\mathrm{d}\Xi,\end{aligned}$$

$i=1,2,3$, and

$$\left\langle\overline{\mathbf{a}}\cdot\mathbf{u}+\bar{A}\right\rangle=0.$$

After determining all parameters in the initial gas distribution function f_0 and the equilibrium state g, and substituting Eq. (3.26) and Eq. (3.27) into Eq. (3.25), the time-dependent distribution function $f(\mathbf{x},t,\mathbf{u},\boldsymbol{\xi})$ at a cell interface can be expressed as

$$\begin{aligned}f(\mathbf{x},t,\mathbf{u},\boldsymbol{\xi})=&c_1g_0+c_2\overline{\mathbf{a}}\cdot\mathbf{u}g_0+c_3\bar{A}g_0\\&+[c_4g^r+c_5\mathbf{a}^r\cdot\mathbf{u}g^r+c_6A^rg^r](1-H(u))\\&+\left[c_4g^l+c_5\mathbf{a}^l\cdot\mathbf{u}g^l+c_6A^lg^l\right]H(u),\end{aligned}\tag{3.28}$$

with coefficients,

$$\begin{aligned}&c_1=1-e^{-t/\tau},\\&c_2=(t+\tau)e^{-t/\tau}-\tau,\\&c_3=t-\tau+\tau e^{-t/\tau},\\&c_4=e^{-t/\tau},\\&c_5=-(t+\tau)e^{-t/\tau},\\&c_6=-\tau e^{-t/\tau}.\end{aligned}$$

Then, the integrated flux transport over a time step can be obtained,

$$\mathbf{F}=\int_0^{\Delta t}\int \mathbf{u}\cdot\mathbf{n}f(\mathbf{x},t,\mathbf{u},\boldsymbol{\xi})\boldsymbol{\psi}\mathrm{d}\Xi\mathrm{d}t, \tag{3.29}$$

where $\mathbf{n}$ is the unit vector in the outer normal direction of the associated cell interface. Then, the cell-averaged conservative variables of cell i can be updated as follows,

$$\mathbf{W}_i^{n+1}=\mathbf{W}_i^n-\frac{1}{\Omega_i}\sum_{S_{ij}\in\partial\Omega_i}\mathbf{F}_{ij}S_{ij}, \tag{3.30}$$

where Ω_i is the volume of cell i, $\partial\Omega_i$ denotes the set of interfaces of cell i, S_{ij} is the area of the cell interface, $\mathbf{F}_{ij}$ denotes the projected macroscopic fluxes in the normal direction, and $\mathbf{W}_g=\left[\widetilde{\rho}_g,\widetilde{\rho}_g\mathbf{U}_g,\widetilde{\rho}_gE_g\right]^T$ are the cell-averaged conservative variables for the gas phase.

With the interactive force between the gas and particle phases, the changes in the momentum and energy of the gas phase can be calculated as

$$\mathbf{W}_g^{n+1}=\mathbf{W}_g+\mathbf{Q}\Delta t, \tag{3.31}$$

where

$$\mathbf{W}_g=\begin{bmatrix}\widetilde{\rho}_g\\ \widetilde{\rho}_g\mathbf{U}_g\\ \widetilde{\rho}_gE_g\end{bmatrix},\quad \mathbf{Q}=\begin{bmatrix}0\\ \frac{\epsilon_s\rho_s(\mathbf{U}_s-\mathbf{U}_g)}{\tau_{st}}+\epsilon_s\nabla_x p_g\\ \frac{\epsilon_s\rho_s\mathbf{U}_s\cdot(\mathbf{U}_s-\mathbf{U}_g)}{\tau_{st}}+3\frac{p_s}{\tau_{st}}+\epsilon_s\mathbf{U}_s\cdot\nabla_x p_g\end{bmatrix}.$$

Finally, the heat conduction between gas flow and solid particle will also affect the temperature of gas flow, which is governed by Eq. (3.22),

$$\frac{\mathrm{d}\left(\widetilde{\rho}_gC_gT_g\right)}{\mathrm{d}t}=-\epsilon_s\rho_sC_s\frac{T_g-T_s^m}{\tau_T}.$$

The temperature of gas phase T_g can be updated by the analytical solution from the above equation. Now the update for the gas phase in one time step has been finished.

With the updates of macroscopic flow variables in the particle and gas phases, the volume fractions ϵ_s and ϵ_g are determined as follows:

1) Update the apparent density of the solid particle phase and gas phase, $\epsilon_s\rho_s$ and $\widetilde{\rho}_g$.

2) The volume fraction of the solid particle phase is given by

$$\epsilon_s=\frac{\epsilon_s\rho_s}{\rho_s},$$

where ρ_s is a material-dependent density of the solid particle.

3) The volume fraction of the gas phase is calculated according to the relation between ϵ_s and ϵ_g,

$$\epsilon_g=1-\epsilon_s.$$

3.3 Limiting solutions for the gas-particle two-phase flow

The limiting cases of the gas-particle two-phase system will be analyzed. In general, the gas-particle flow regime is determined by two dimensionless numbers, i.e., the Knudsen number Kn_s and Stokes number St_s. The Knudsen number is defined by the ratio of collision time of solid particle to the characteristic time of macroscopic flow,

$$Kn_s = \frac{\tau_s}{t_{ref}}. \tag{3.32}$$

Specifically, τ_s is the time interval between collisions of solid particles, or called the relaxation time of the particle phase. According to the previous studies [40, 45], in this paper τ_s is taken as

$$\tau_s = \frac{\sqrt{\pi} d_s}{12 \epsilon_s g_0} \sqrt{2\lambda_s}, \tag{3.33}$$

where d_s is the diameter of solid particle, ϵ_s is the volume fraction of solid phase, and $\lambda_s = \frac{1}{2RT_s}$ is related to the granular temperature of solid phase T_s. g_0 is the radial distribution function with the following form,

$$g_0 = \frac{2-c}{2(1-c)^3}, \tag{3.34}$$

where $c = \epsilon_s / \epsilon_{s,\max}$ is the ratio of the volume fraction ϵ_s to the maximum allowed volume fraction of the solid phase $\epsilon_{s,\max}$. In the dilute regime, $\epsilon_s \ll \epsilon_{s,\max}$, which leads to $c \to 0$ and $g_0 \to 1$. On the contrary, when $\epsilon_s \to \epsilon_{s,\max}$, we have $g_0 \to \infty$ and $\tau_s \to 0$ for the highly dense particle flow. In this paper, we mainly focus on dilute flow, and therefore g_0 can be neglected. Besides, t_{ref} is the characteristic time scale, which is defined as the ratio of the flow characteristic length to the flow characteristic velocity, $t_{ref} = L_{ref}/U_{ref}$. Kn_s determines the flow regime of the particle phase. When Kn_s is very large, i.e., $\tau_s \to \infty$, the collision time is much larger than the characteristic time scale, and no particle-particle collision occurs. In this limit, the fluxes associated with wave, such as $\mathbf{F}_{ij}^{eq}$ and $\mathbf{F}_{ij}^{fr,wave}$ in Eq. (3.16), become zero. Therefore, the collisionless particle transport solution with the interaction with the gas phase alone is obtained by UGKWP, the so-called EL method. On the contrary, when Kn_s is very small, i.e., $\tau_s \to 0$, the particle phase will go to the continuum flow regime and only the wave part will be left in the update of solutions in Eq. (3.16). The limiting scheme will become EE method.

Another dimensionless number St_s is defined by

$$St_s = \frac{\tau_{st}}{t_{ref}}, \tag{3.35}$$

where τ_{st} is the particle internal response time, which can be obtained from the drag force, and t_{ref} is the same with the above definition. St_s determines the interactive coupling

between the particle phase and gas phase. When St_s is very large, i.e., $\tau_{st} \to \infty$, the drag fore term **D** is nearly zero, where the particle phase is decoupled from the gas phase. In this case, the particle phase cannot be driven by the gas flow and PTC phenomena will occur. On the other hand, a small $St_s \to 0$ leads to $\mathbf{u} \to \mathbf{U}_g$, where the solid particle will have the same velocity as the gas flow. Then, a single mixture phase is formed and its evolution can be modeled by the fluid dynamic equations.

4 Numerical tests

4.1 Wind sand shock tube problem

The 1D wind sand shock tube problem in different particle regimes is tested to show the multiscale solution from GKS-UGKWP. The initial condition is

$$(\epsilon_s\rho_s, U_s, p_s, T_s^m) = \begin{cases} (0.5,0,0.75,1.0), & 0 \le x \le 0.5, \\ (0.5,0,0.75,0.8), & 0.5 < x \le 1, \end{cases}$$

for the solid particle phase, and

$$(\epsilon_g\rho_g, U_g, p_g) = \begin{cases} (1,0,1), & 0 \le x \le 0.5, \\ (0.125,0,0.1), & 0.5 < x \le 1, \end{cases}$$

for the gas phase. The computational domain is $[0,1]$ and the mesh number is 100. The non-dimensional heat capacity of particle phase and gas phase is $C_s = 0.1$ and $C_g = 0.2$, respectively. The relaxation time of the heat conduction τ_T between gas flow and solid particle is assumed as 0.1. In this case, the collision between solid particles are assumed as elastic collision, i.e., $r = 1$, and the gravity is neglected. The target of this case is to validate the ability of the UGKWP to recover the solutions of TFM and particle method in different limiting flow regimes for the particle phase. Firstly, the flow in high particle collision regime with $Kn_s = 10^{-5}$ is studied, where the solid particle is in the continuum flow regime with local equilibrium distribution determined by the macroscopic variables. Therefore, the method based on macroscopic flow variables, such as TFM, could also give the correct solution in this situation for the evolution of particle phase. The particle internal response time is assumed to be a constant $\tau_{st} = 0.1$. The results from the GKS-UGKWP and TFM are presented in Fig. 1, where good agreements have been obtained in the highly collisional regime. Then, another limit of the collisionless regime is tested by assuming an infinity solid phase Knudsen number Kn_s. In this regime, no inter-particle collision exists and the solid particle keeps free transport. In this case, a large particle internal response time $\tau_{st} = 0.2$ is taken. The results from the MP-PIC method and GKS-UGKWP are shown in Fig. 2, where identical solutions are obtained in the collisionless regime.

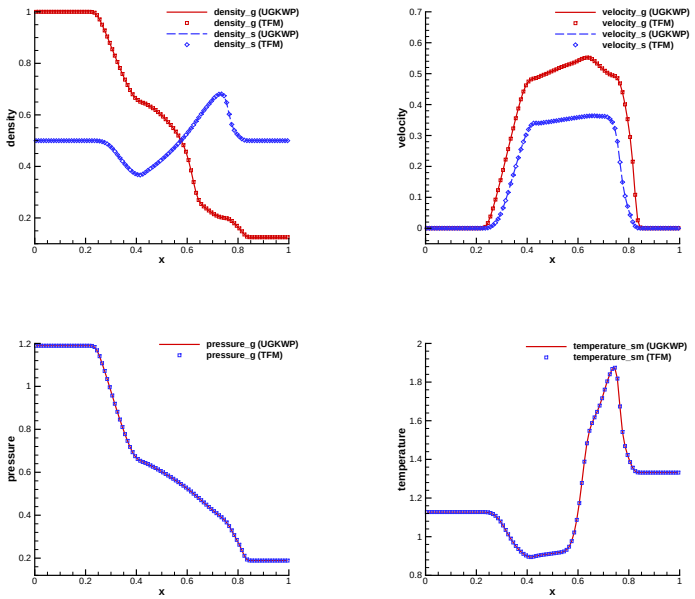

Figure 1: Wind sand shock tube problem in highly collisional regime. Solutions from the GKS-UGKWP and TFM at $t=0.2$, $Kn_s=10^{-5}$, $\tau_{st}=0.1$, and $\tau_T=0.1$. Apparent densities of gas and particle phase, velocities of gas and particle phase, pressure of gas phase, and material temperature of solid particles are included.

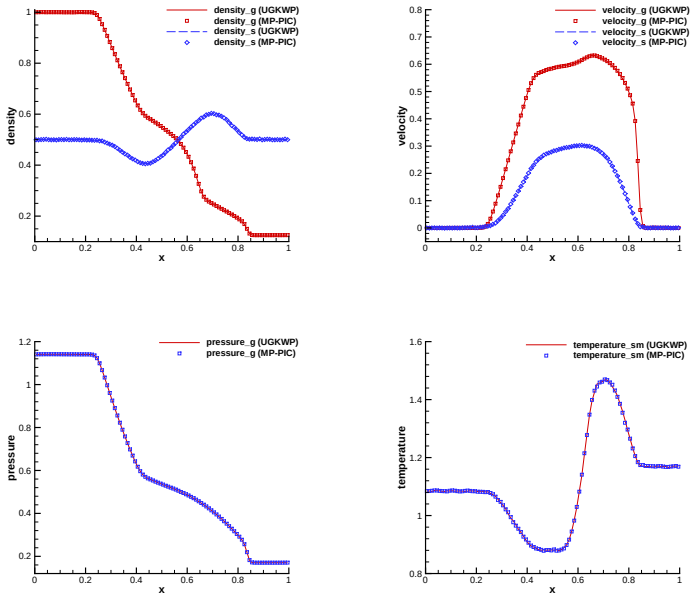

Figure 2: Wind sand shock tube problem in the collisionless regime. Solutions by the GKS-UGKWP and MP-PIC method at $t=0.2$, $Kn_s=\infty$, $\tau_{st}=0.2$, and $\tau_T=0.1$. Apparent densities of gas and particle phase, velocities of gas and particle phase, pressure of gas phase, and material temperature of solid particles are included.

4.2 Impinging particle jets problem

A significant non-equilibrium behavior of gas-particle flow is the particle trajectory crossing (PTC), which occurs in the collisionless regime [40]. It is easy to understand that if no collision exists, all the solid particles will keep their initial velocity and thus cross with each other at the meeting location. In contrast, in a finite Kn number, the collision between particles will lead to the multiply particle velocities, and get particle cloud scattering. Here, two particle jets impinging problems are tested for the performance of the UGKWP in the capturing of the above representative phenomena of particle flow. The associated sketch is given in Fig. 3. The whole computational domain is $L\times H=9cm\times 6cm$ and a uniform grid with 180×120 mesh points is used. Initially, two particle beams with an inlet width $x=0.6cm$ at the up and down boundaries symmetrically enter the computational domain. The angle between particle beam and the boundary is 135° and the length of particle beam is $0.424cm$. Besides, the absolute velocity of particle beam is $|\mathbf{U}|=1m/s$, and the granular temperature T_s is zero. The reference time in this case is taken as $t_{ref}=L/U$. The reflection boundary condition is employed at the up and down boundaries except at the inlet of the impinging particle beam. The right boundary has the outflow boundary condition. In this case, the interaction between particle phase and gas phase is neglected and thus only the particle phase is simulated by UGKWP.

The collisionless regime is studied first at $Kn_s=\infty$. In this regime, the solid particle will keep the initial velocity until they meet the wall. Fig. 4 shows PTC and wall reflection exactly. Since no collision exists, both the elastic collision and inelastic collision models show the same result. Then, at $Kn_s=1$ with the influence of both transport and collision, the results from the elastic collision model are shown in Fig. 5. Due to the effect of elastic particle-particle collisions, the solid particles will show scatting at the encountering zone of two impinging jets. In contrast, for the inelastic collision, the particles will get together

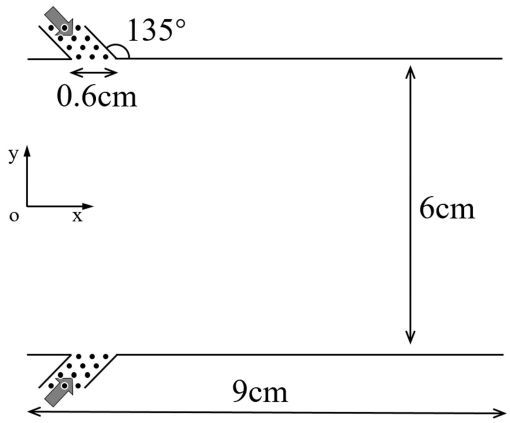

Figure 3: The sketch of particle jets impinging problem.

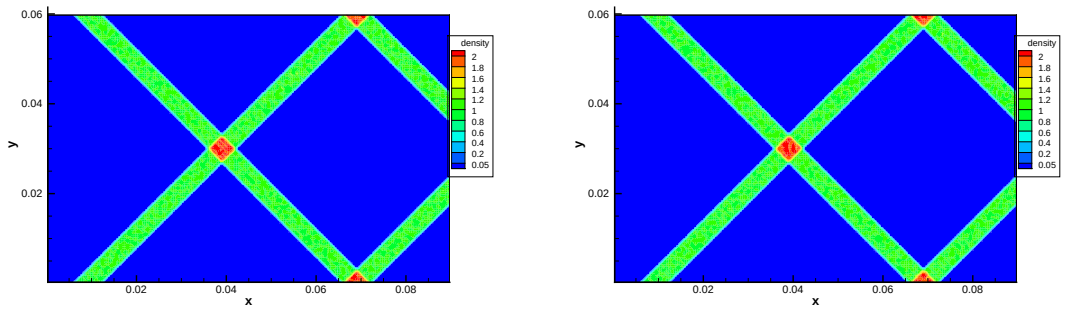

Figure 4: Apparent density for impinging particle jets by the UGKWP in collisionless regime with $Kn=\infty$ at $t=0.12$. The left figure is elastic collision and the right is inelastic collision.

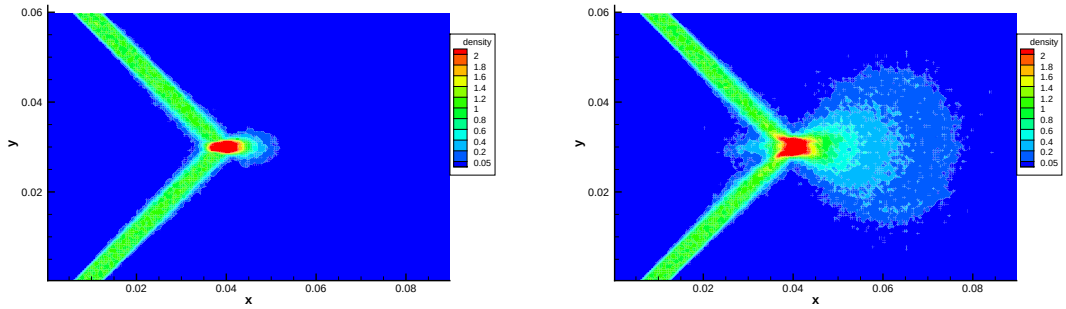

Figure 5: Apparent density for the impinging particle jets by UGKWP with $Kn=1$ at $t=0.05$ and $t=0.08$ from elastic collision model.

after collision and move horizontally to the right, as shown in Fig. 6. During this process, the granular temperature is lost in the inelastic collision, and the post-collision particles have the same velocity.

At the Knudsen number $Kn_s=10^2$, the solutions are shown in Fig. 7. For the elastic particle collision, besides the scattering, a small portion of particles still keep their initial velocity, which is not found in the solution at $Kn_s=1$. In comparison with $Kn_s=1$ case, the free transport of particles at $Kn_s=10^2$ will play a significant role on the particle evolution. The same phenomenon can be obtained more obviously in the inelastic collision case. Fig. 7 shows clearly the effect from the particle free transport and collision at such a Knudsen number.

4.3 Particle distribution in Taylor-Green vortex flow field

The preferential concentration of dispersed particles in gas-particle two-phase flow is investigated. In general, the particles prefer to concentrate in the region at low gas vor-

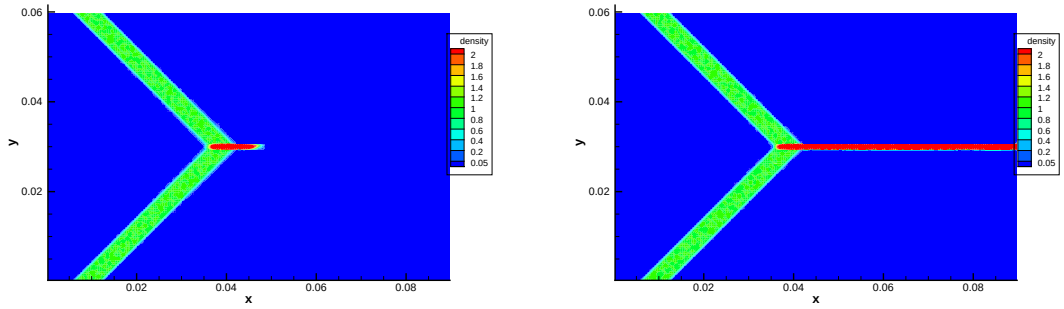

Figure 6: Apparent density for the impinging particle jets by the UGKWP with $Kn=1$ at $t=0.05$ and $t=0.12$ from inelastic collision model.

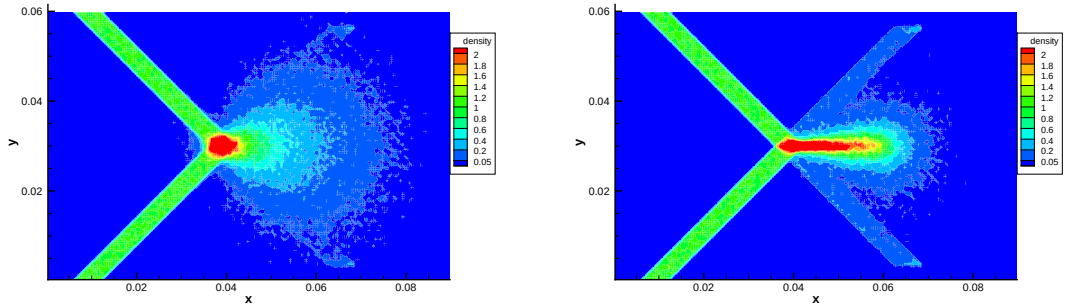

Figure 7: Apparent density for the impinging particle jets by the UGKWP with $Kn=10^2$ at $t=0.08$. The left figure is elastic collision and the right is inelastic collision.

ticity [12, 13]. The two-dimensional Taylor-Green vortex flow is chosen for the gaseous flow field. Two initial conditions are considered, which are shown in Fig. 8. For Type 1, the solid particles are uniformly distributed initially in the whole computational domain,

$$\rho_g=1.0,\quad U_g=\cos(2\pi x)\sin(2\pi y),\quad V_g=-\sin(2\pi x)\cos(2\pi y),$$
$$p_g=10.0+[\cos(4\pi x)+\cos(4\pi y)]/4,$$

for the gas phase, and

$$\epsilon_s\rho_s=1.0,\quad U_s=U_g,\ V_s=V_g,\quad T_s=1.0^{-8},$$

for the solid particle phase. While for Type 2, the solid particles are uniformly located within a circular region centered at $(0.5,1-1.25/\pi)$ with radius $r=0.25/\pi$, and the gaseous flow field is shifted with a distance of 0.5π in both directions in comparison with Type 1. For both initial conditions, the computational domain is $[0,1]\times[0,1]$ covered by 100×100 uniform grids. The periodic boundary condition is employed for all boundaries.

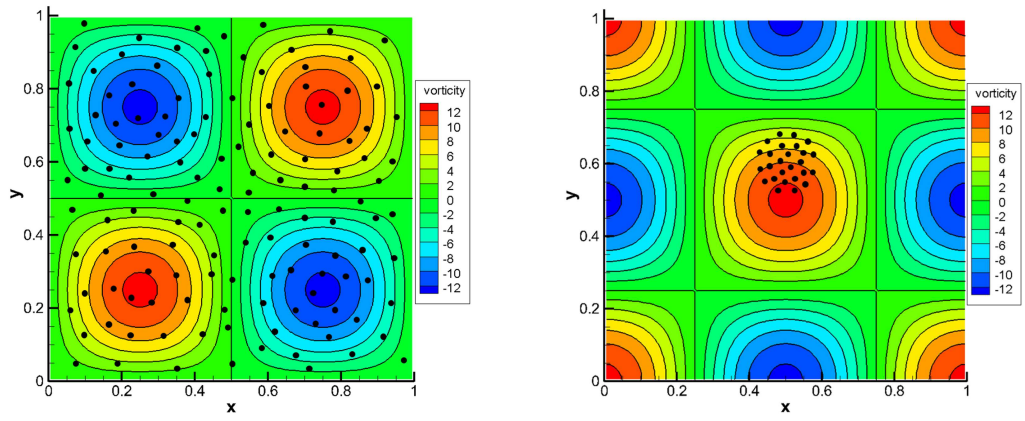

Figure 8: The sketch of the initial distribution of apparent density of solid phase (black points) and the initial vorticity of gas phase (contours). The left figure is Type 1 and the right figure is Type 2.

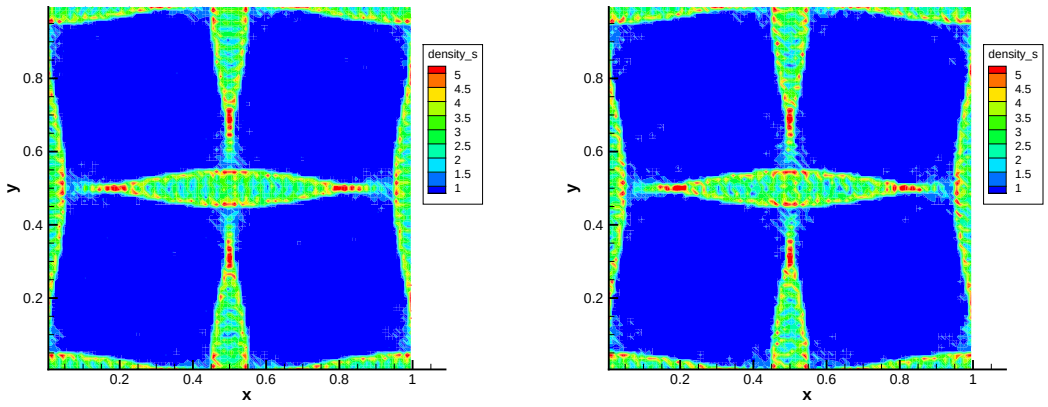

Figure 9: Apparent density of the particle phase for Taylor-Green vortex problem in the collisionless regime with $Kn_s=10^4$ and $St=0.3$ at $t=0.3$. Left: UGKWP solution; Right: MP-PIC solution.

The Reynolds number of gas phase is taken as $Re=400$, which leads to $\mu=2.5\times10^{-3}$. The reference time is taken as $t_{ref}=1$ for this test case. According to the previous research, the critical Stokes number is $St_c=1/(8\pi)$ [12]. If the Stokes number below St_c, the particle will concentrate around the low vorticity area; while if the Stokes number is larger than St_c, the particle trajectory crossing will occur.

For the Type 1 initial condition, firstly we consider a collisionless regime with $Kn_s=10^4$. At $St=0.3$, the apparent density of solid phase at $t=0.3$ and $t=2.5$ are shown in Fig. 9 and Fig. 10, respectively. When $St=0.3>St_c$, the velocity of particle-phase will not keep mono-kinetic and the particle trajectory crossing will occur accordingly.

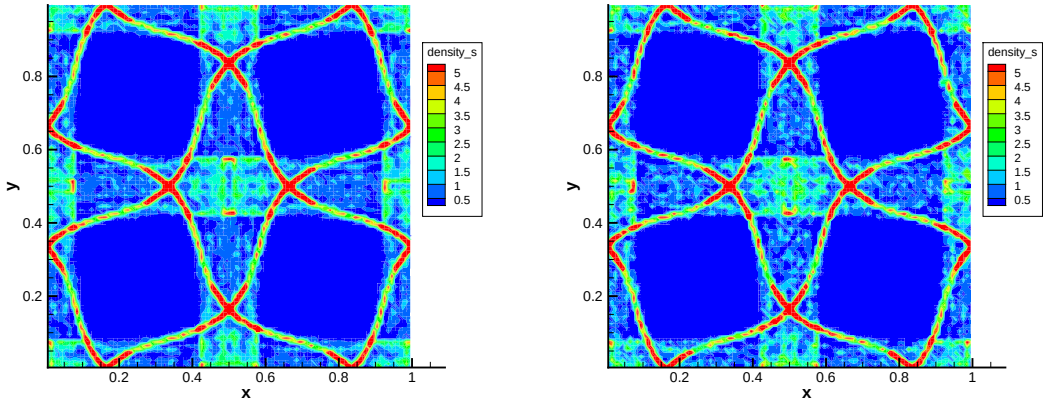

Figure 10: Apparent density of the particle phase for Taylor-Green vortex problem in the collisionless regime with $Kn_s=10^4$ and $St=0.3$ at $t=2.5$. Left: UGKWP solution; Right: MP-PIC solution.

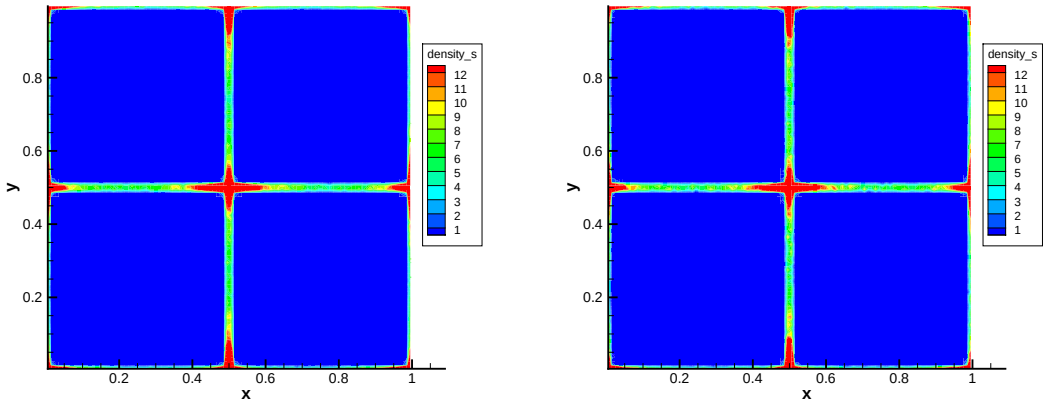

Figure 11: Apparent density of the particle phase for Taylor-Green vortex problem in the collisionless regime with $Kn_s=10^4$ and $St=0.039$ at $t=2.5$. Left: UGKWP solution; Right: MP-PIC solution.

In contrast, when $St=0.039<St_c$, the solid particles will concentrate at low vorticity region, as presented in Fig. 11. In this regime, both the UGKWP and MP-PIC give the same solutions. Then, at $Kn_s=10^{-6}$ and $St=0.3$, the effect of collision is dominant in the determination of the evolution results. When the inelastic collision is employed for the particle-particle collision, the granular temperature will get lost after collision and thus post-collision particles will have the same velocity. All particles will accumulate and move towards to the low-vorticity region even though $St=0.3$ is larger than St_c, as shown in Fig. 12. In this highly collisional regime, the results by TFM are also presented and show the same solutions as that from UGKWP.

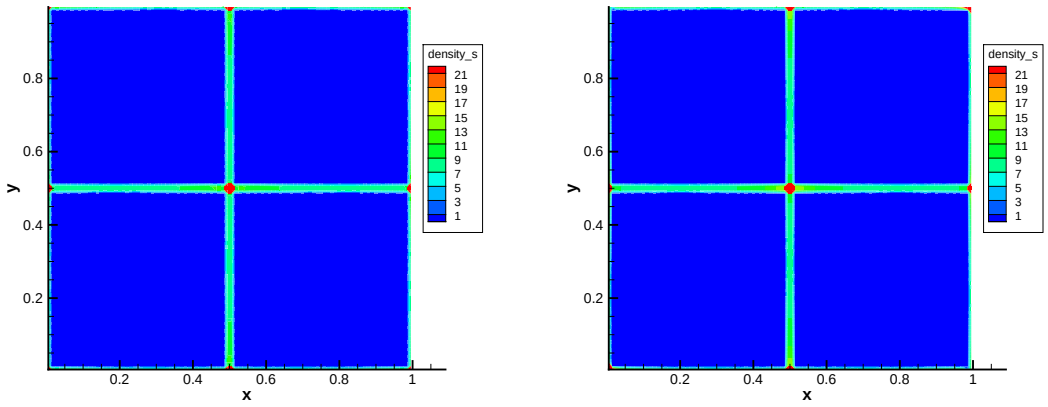

Figure 12: Apparent density of the particle phase for Taylor-Green vortex problem in the high collision regime with $Kn_s=10^{-6}$ and $St=0.3$ at $t=0.6$. Left: UGKWP solution; Right: TFM solution.

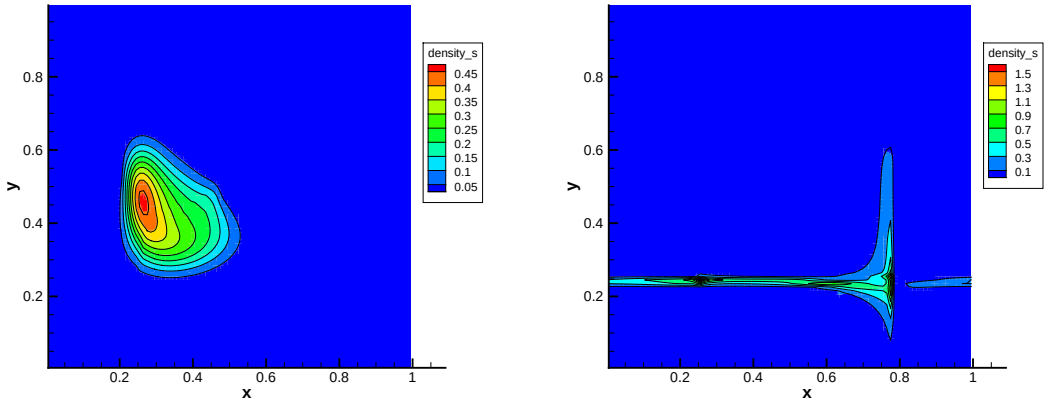

Figure 13: Apparent density of the particle phase for Taylor-Green vortex problem in the high collision regime with $Kn_s=10^{-6}$ and $St=0.1$ at $t=0.5$ (left) and $t=1.2$ (right) for UGKWP (flood) and TFM (line).

For the Type 2 initial condition, in the highly collision regime the Knudsen number $Kn_s=10^{-6}$ and two Stokes numbers $St=0.1$ and $St=0.001$ are considered and the results are given in Fig. 13 and Fig. 14. The same conclusion as Type 1 case can be made. When $St<St_c$, the solid particles will stay in the original vortex and PTC will not occur. When $St>St_c$, the solid particles will have the ability to escape from the original vortex region and enter the neighboring one. In the highly collisional regime, the results by TFM and UGKWP are consistent.

The comparison between UGKS and UGKWP for the dilute gas-particle flow is conducted through the Taylor-Green vortex problem in the following. Two typical cases,

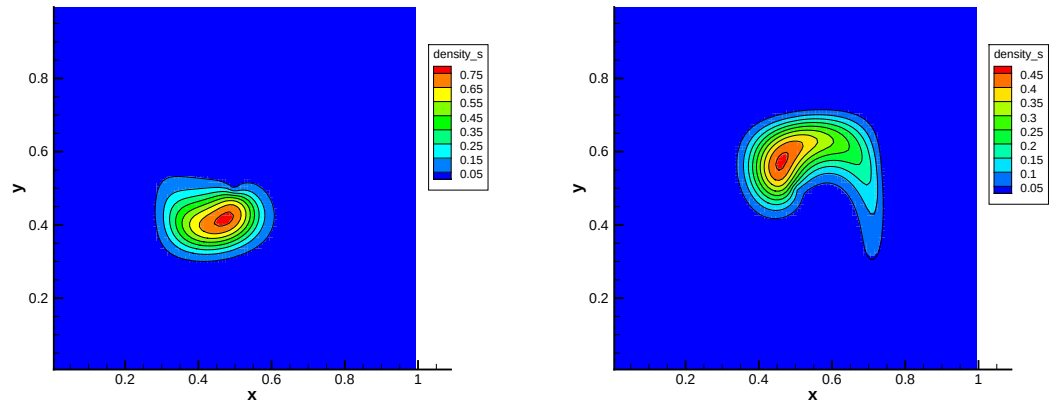

Figure 14: Apparent density of the particle phase for Taylor-Green vortex problem in the high collision regime with $Kn_s=10^{-6}$ and $St=0.001$ at $t=0.5$ (left) and $t=1.2$ (right) from UGKWP (flood) and TFM (line).

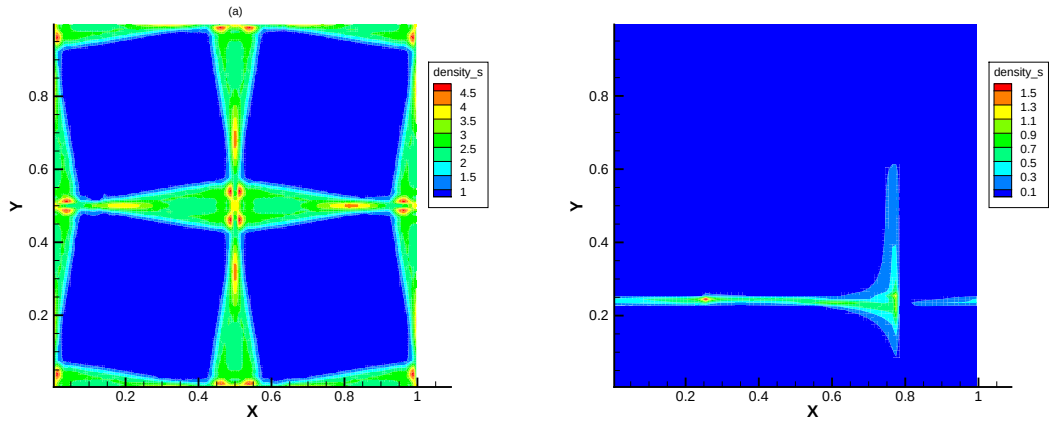

Figure 15: Apparent density of the particle phase for Taylor-Green vortex problem by UGKS. (a) The particle phase is in the collisionless regime with $Kn_s=10^4$, $St=0.3$, and Type 1 initial condition at $t=0.3$. (b) The particle phase is in the high collision regime with $Kn_s=10^{-6}$, $St=0.1$, and Type 2 initial condition at $t=1.2$.

including the collisionless regime and highly collision regime, are considered. Firstly, the particle phase is in the collisionless regime with $Kn_s=10^4$ and $St=0.3$, and Type 1 initial condition, the result by UGKS in a domain with 150×150 mesh points at $t=0.3$ is shown in Fig. 15(a). Compared with the result by UGKWP in Fig. 9, it shows that the UGKWP has a higher resolution even with a coarser mesh than that from UGKS. When refining the mesh, the solution from UGKS can be improved [29]. Besides, at a long running time, both UGKWP and UGKS can give correct prediction of particle behavior. Similar flow pattern was also obtained by others, e.g., Figure 5 in [12]. Secondly, for the highly colli-

Table 1: Computation efficiency of UGKS and UGKWP in collisionless regime, evaluated on a machine of single Intel core i7-9700@3.00 GHz.

	Physical space	Velocity space	CPU time	Ratio
UGKS	150×150	42 × 42	2 h 47 min	55.7
UGKWP	100×100	10	3 min	—

Table 2: Computation efficiency of UGKS and UGKWP for high collision regime, evaluated on a machine of single Intel core i7-9700@3.00 GHz.

	Physical space	Velocity space	CPU time	Ratio
UGKS	100×100	32 × 32	18 min 39 s	27.3
UGKWP	100×100	0	41 s	—

sion regime with $Kn_s = 10^{-6}$, $St = 0.1$, and Type 2 initial condition, the result of UGKS at $t = 1.2$ is shown in Fig. 15(b), which agrees well the result by UGKWP in Fig. 13. Under this regime, both UGKS and UGKWP can give the same prediction as the Eulerian TFM approach. The above results indicate that both UGKS and UGKWP can give accurate prediction for the evolution of particle flow in different regimes, and validate their ability in simulating disperse dilute gas-particle flow. Both UGKS and UGKWP are based on the identical multiscale transport modeling for the particle flow, but with DVM and wave-particle discretization, respectively. For efficiency, due to the absence of discrete particle velocity space UGKWP performs much better than UGKS in both collisionless and highly collisional regime, as shown in Table 1 and Table 2.

4.4 Upward particle-laden jet into a cross-flow

The 2D upward particle-laden jet into a cross-flow is studied for the gas-particle system. Many investigations about the interaction between the upward jet and the cross-flow have been conducted under different conditions [20, 44, 47]. This problem is challenging when the upward jet carries solid particles. Fig. 16 shows a sketch of the simulated problem. A mixed gas particle-laden jet is injecting from the bottom of the computational domain. The diameter of the upward jet is $D_{jet} = 4.62mm$ and it is located at $10D_{jet}$. The whole computational domain $L \times H$ is $100D_{jet} \times 80D_{jet}$. The density and diameter of the solid particles carried by the upward gas jet are $\rho_s = 2638kg/m^3$ and $d_s = 15\mu m$, respectively. Initially, the volume fraction ϵ_s of particle phase in the upward jet is 0.0087, and the corresponding apparent density $\epsilon_s\rho_s$ is $22.95kg/m^3$. The jet velocity of the upward gas V_{jet} is $26.38m/s$ and the solid particle has the same velocity as the gas initially. The density of the gas in the jet is $1.21kg/m^3$. The gravity for the solid particles is $9.8m/s^2$. The initial granular temperature of solid particle phase T_s is assumed to be zero. The cross-flow, or called main flow in the domain, moves from left to right with density $1.1kg/m^3$ and temperature $298K$. The velocity of main flow U_∞ is $16.80m/s$, which leads to a veloc-

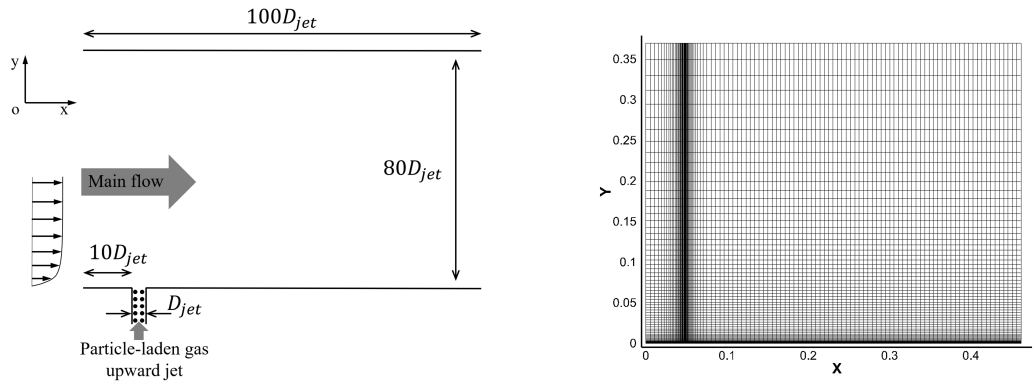

Figure 16: The sketch and mesh of the test for the upward particle-laden jet in a cross flow field.

ity ratio $V_{jet}/U_\infty = 1.57$. A non-uniform mesh with 120×65 grid points is used, which is shown in Fig. 16. The mesh is refined in the region near the wall and the upward jet, and the size of the first layer mesh is set as $0.20mm$. Non-slip wall boundary condition is applied for bottom boundary except at the upward jet region, and free boundary condition is used for both right and up boundaries. The reference time t_{ref} is defined as the ratio of the height of the computational domain to the upward jet velocity H/V_{jet}. The Stokes number is about 0.12 and the Knudsen number $Kn_s = 1.1\times 10^{-2}$ for the initial particle phase. Considering that the gas phase flow is turbulent, the $k-\omega$ SST turbulence model is employed for the gas flow [41].

In this study, the cross flow and the gas in the jet will be calculated by the GKS with turbulence model. The movement of the solid particles in the jet will be controlled by their interaction with the gas and their inner solid particle collision. The influence on the gas phase from the solid particle is ignored. In other words, this test is mainly about the evolution of solid particles under the external gas field. Note that the collisions between solid particles will also have dynamic effect on the solid particle evolution. The density and streamline of the gas flow at $t = 0.1s$ are presented in Fig. 17, where a large vortex is formed due to the interaction between the upward gas jet and the main flow. In order to compensate the lost dispersion effect due to the under-resolved vortex in the turbulent gas phase simulation, the turbulence dispersion force is added in the particle phase, where the model proposed by Lahey is employed [26],

$$F_T = -C_T \rho_g k_g \nabla \epsilon_s,$$

where C_T is taken as 0.1, and k_g is the turbulence kinetic energy of the gas flow. The apparent density of particle phase at $t = 0.1s$ with $St = 0.12$ is shown in Fig. 18. As stated earlier, the UGKWP simulates the particle phase by both wave and particle, where their separate components are shown in Fig. 18(b) and Fig. 18(c). Fig. 18(a) shows the total apparent density of the particle phase, which is the sum of the wave and particle contributions. The results show that wave and particle are distributed adaptively. In the

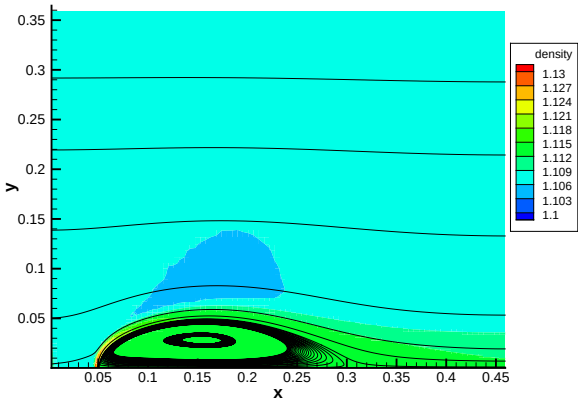

Figure 17: The density and streamline of gas phase at $t=0.1s$ calculated by the GKS with k-ω SST turbulence model.

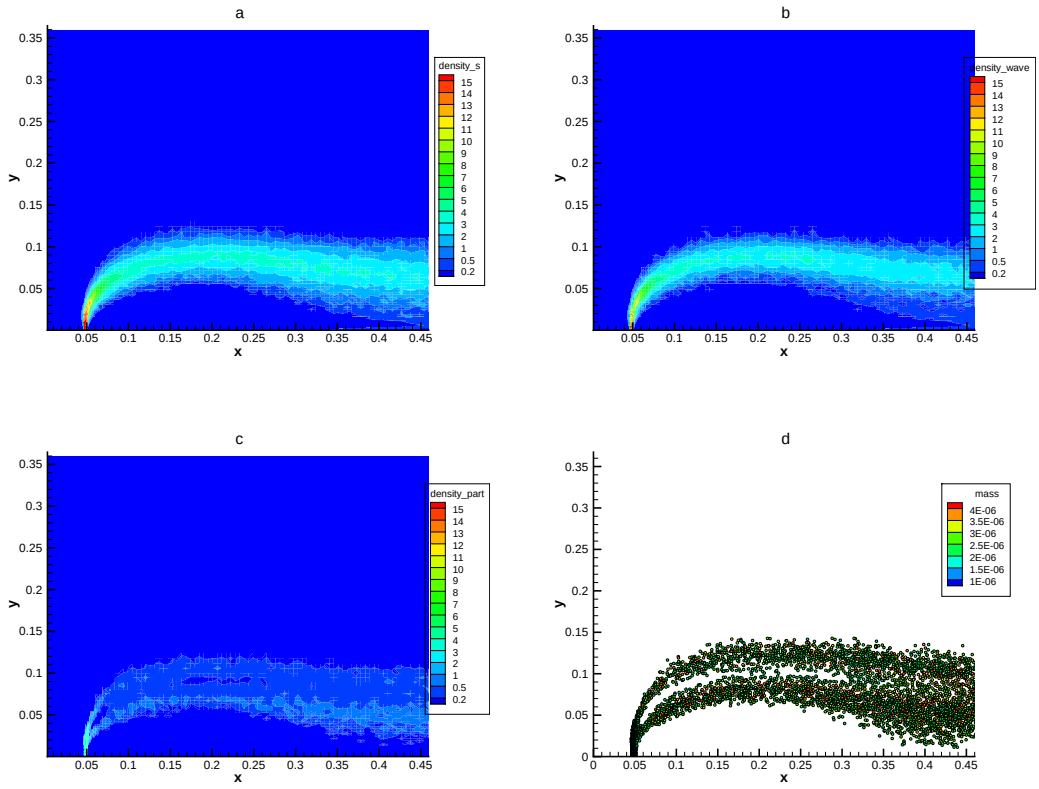

Figure 18: The apparent density of solid particle phase at $t=0.1s$ with $St=0.12$ calculated by GKS-UGKWP. (a) total apparent density of particle phase; (b) apparent density calculated by wave; (c) apparent density calculated by particle; (d) the scatter plot of sampled particles.

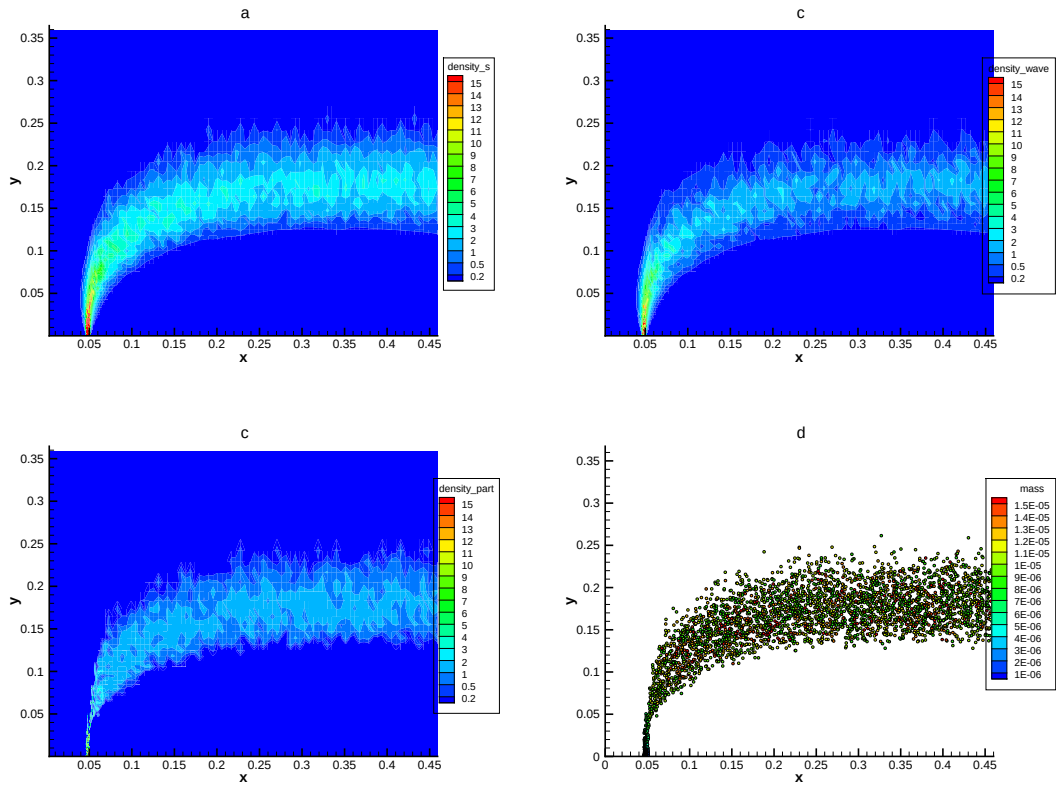

Figure 19: The apparent density of solid particle phase at $t=0.1s$ with $St=1.2$ calculated by GKS-UGKWP, (a) total apparent density of particle phase; (b) apparent density calculated by wave; (c) apparent density calculated by particle; (d) the scatter plot of sampled particles.

core region of particle phase, there are more collisions between solid particles and a high representation of density goes to wave automatically in UGKWP. Furthermore, Fig. 18(d) shows the sampled particles in the simulation, which appear more on the edges of particle phase with less particle-particle collision and these particles have the corresponding density distribution shown in Fig. 18(c). The solid particles in the jet change their velocities and movement towards to the right due to their interaction with the horizontal cross flow and gas inside the jet. Similar results have been found in the previous study [47]. The dispersion effect is caused by the complex interaction between solid particle-gas interaction and particle-particle collisions. With the increase of particle diameter d_s, a large Stokes number $St=1.2$ can be achieved, which is about 10 times of the previous Stokes number. With the Knudsen number $Kn_s=3.4\times10^{-2}$ for the particles in the jet, the simulation results are shown in Fig. 19. Since a large St means a weak interaction between the solid particle and the gas phase, the solid particles in the jet can move to a higher vertical position, and are pushed to the right by the gas flow. Furthermore, in comparison with

Fig. 18, the wave part in this case takes a lower percentage in the particle representation due to a larger Knudsen number.

4.5 Particle bed fluidization in shock tube

The fluidization of a particle bed induced by a shock wave is a challenging problem for the numerical simulation [22, 48, 50]. This is a complicated physical problem since it involves the movement of solid particles, the interaction of solid particles with the shock, the reflection and transmission of a shock. In this example, the experiment conducted by Rogue is simulated by the GKS-UGKWP [48]. Fig. 20 shows a sketch of this experiment. Initially, a particle bed is located at $15cm$ in the vertical direction. This particle bed is comprised of a group of glass particles with the diameter $1.5mm$, and the thickness of this particle bed is $2cm$. Besides, the density of solid particles is $2500kg/m^3$, and the volume fraction ϵ_s of the solid particle bed is 0.65. The initial density and pressure of the gas in the tube are $1.2kg/m^3$ and 10^5Pa. A shock of Mach number 1.3 is created by the high-pressure gas with vertical velocity $V_0 = 151m/s$ at the inlet boundary. Two pressure gauges are set at the upstream and the downstream, $11.0cm$ below the particle bed and $4.3cm$ above the particle bed, to monitor the instantaneous pressure change. The computational domain $L \times H$ is $1cm \times 90cm$ covered by 10×900 uniform cells. Considering that the turbulence intensity of the gas will increase after the interaction with a particle bed, the turbulence energy is regarded as the internal energy and thus the internal degree of freedom of the gas phase will be modeled by $k(t) = k_0 + 1.5 \times (t/t_{end})^3$. In this case, the reference time t_{ref} is defined as the ratio of the whole tube length H to the inflow gas velocity V_0. The Stokes number is approximately $St = 0.62$ and the Knudsen number of the particle phase is around $Kn_s = 2 \times 10^{-3}$. The comparison of the numerical result by

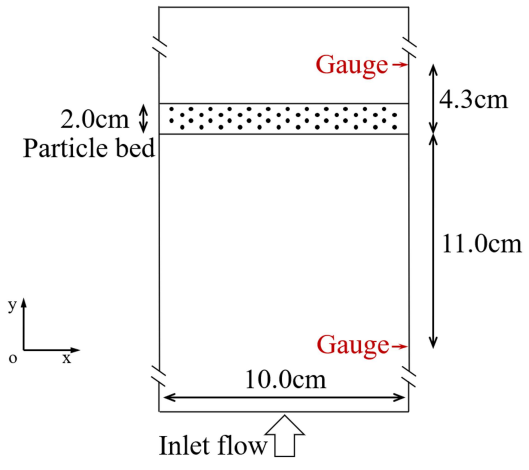

Figure 20: The sketch of the induced fluidization of a particle bed by a shock wave.

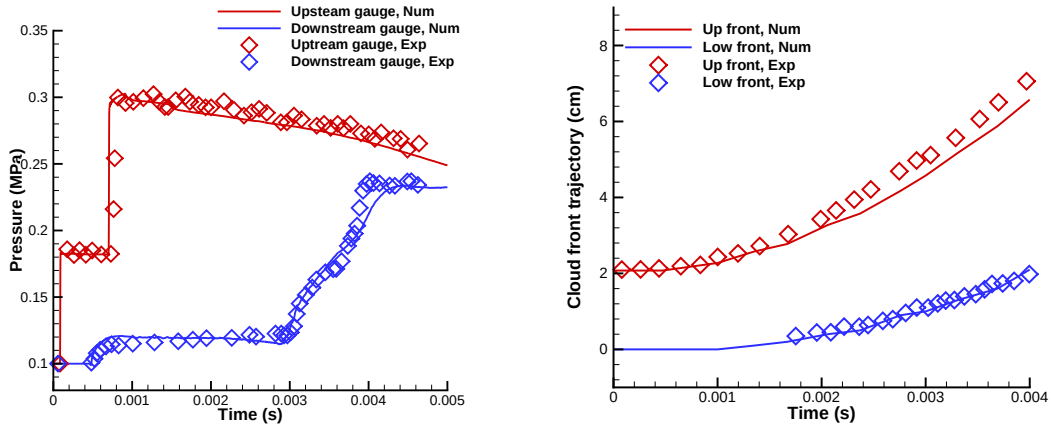

Figure 21: Numerical results by GKS-UGKWP and experiment data for particle bed fluidization problem. The left figure shows the time-dependent pressure at two gauge positions and the right figure is about the trajectory evolution of upper and lower fronts of solid particle cloud.

the GKS-UGKWP with experiment data is shown in Fig. 21. The instantaneous pressure values at the upstream and downstream gauges indicate that both the reflected shock and transmitted shock are obtained correctly. In addition, the upper and lower fronts of the solid particle cloud also agree well with the experiment data.

5 Conclusion

The modeling and simulation of gas-particle two-phase flow is challenging in computational fluid dynamics. The flow physics of the solid particle can manifest a variety of dynamics in different regimes. With the variation of particle Knudsen number, the particle movement can cover dynamics from the macroscopic fluid modeling to the highly non-equilibrium particle free transport. The development of multiscale method becomes necessary. In this paper, a multiscale GKS-UGKWP method has been developed for the disperse dilute gas-particle system. The GKS, as an efficient kinetic theory-based Navier-Stokes solver, is used for the computation of the gas flow. On the other hand, the particle flow in different flow regimes is simulated by the UGKWP, which dynamically decomposes and follows the solid particle phase by discrete particle for the particle free transport and accumulating wave for the equilibrium flow evolution. The multiscale dynamics between the particle free transport in the highly rarefied regime and the NS solution in the continuum flow regime is recovered seamlessly by UGKWP with an adaptive particle and wave composition. At the same time, the momentum and energy exchanges between the gas and particle phase are included in GKS-UGKWP through the coupled evolution of the two phase system. The advantages of using UGKWP for the solid particle phase

evolution is that an efficient approach will be automatically adapted locally according to the local Knudsen number. The proposed method can recover the Eulerian-Eulerian formulation, such as TFM, in the highly collisional regime for the gas-particle system, and the Eulerian-Lagrangian model, such as MP-PIC, in the collisionless regime of the particle phase. Many numerical tests in different regimes have been conducted to validate the proposed method. As a continuous effort, the construction of two-phase GKS-UGKWP for both dilute and dense solid particle phases is under investigation.

Acknowledgments

The current research is supported by National Numerical Windtunnel project, National Science Foundation of China (11772281, 91852114,12172316), Hong Kong research grant council 16208021, and Department of Science and Technology of Guangdong Province (Grant No.2020B1212030001).

Appendix A: Governing equations for the particle phase in the continuum flow regime

The kinetic equation for the particle phase is

$$\frac{\partial f_s}{\partial t}+\nabla_x\cdot(\mathbf{u}f_s)+\nabla_u\cdot(\mathbf{a}f_s+\mathbf{G}f_s)=\frac{g_s-f_s}{\tau_s}, \tag{A.1}$$

and the collision term should satisfy the following compatibility condition when $r=1$,

$$\int\frac{g_s-f_s}{\tau_s}\boldsymbol{\psi}\mathrm{d}\Xi=0,$$

with $\boldsymbol{\psi}=\left(1,\mathbf{u},\frac{1}{2}\left(\mathbf{u}^2+\boldsymbol{\xi}^2\right)\right)^T$.

The drag force $\mathbf{D}$ and buoyancy $\mathbf{F}_b$ are included in $\mathbf{a}$,

$$\mathbf{a}=\frac{\mathbf{U}_g-\mathbf{u}}{\tau_{st}}-\frac{1}{\rho_s}\nabla_x p_g.$$

In the continuum regime, f_s can be expanded as

$$f_s=g_s-\tau_s Dg_s+\tau_s D(\tau_s Dg_s)+\cdots,$$

where $D\phi=\frac{\partial\phi}{\partial t}+\frac{\partial(u_i\phi)}{\partial x_i}+\frac{\partial(a_i\phi+G_i\phi)}{\partial u_i}$. Under the zeroth-order truncation for f_s, i.e., $f_s=g_s+\mathcal{O}(\tau_s)$, and substituting it into Eq. (A.1) and taking moments $\boldsymbol{\psi}$, we have

$$\int\boldsymbol{\psi}\left[\frac{\partial g_s}{\partial t}+\frac{\partial(u_i g_s)}{\partial x_i}+\frac{\partial(a_i g_s+G_i g_s)}{\partial u_i}\right]\mathrm{d}\Xi=0, \tag{A.2}$$

with $a_i=\frac{U_{g,i}-u_i}{\tau_{st}}-\frac{1}{\rho_s}\frac{\partial p_g}{\partial x_i}$. For brevity, the following notation is introduced,

$$<\cdots>=\int(\cdots)g_s\mathrm{d}\Xi.$$

The acceleration term becomes

$$\begin{aligned}\mathcal{A}_i &\overset{def}{=}\frac{\partial(a_ig_s+G_ig_s)}{\partial u_i}\\ &=g_s\frac{\partial(a_i+G_i)}{\partial u_i}+(a_i+G_i)\frac{\partial g_s}{\partial u_i}\\ &=-\frac{1}{\tau_{st}}g_s-2\lambda_s(u_i-U_{s,i})(a_i+G_i)g_s\\ &=-\frac{1}{\tau_{st}}g_s-2\lambda_s(u_i-U_{s,i})\left(\frac{U_{g,i}}{\tau_{st}}-\frac{1}{\rho_s}\frac{\partial p_g}{\partial x_i}+G_i\right)g_s+2\lambda_s\frac{u_i^2-u_iU_{s,i}}{\tau_{st}}g_s,\end{aligned}$$

and the moments relevant to $\mathcal{A}_i$ can be obtained as

$$\begin{aligned}&<\mathcal{A}_i>=0,\\ &<u_j\mathcal{A}_i>=\frac{\epsilon_s\rho_s(U_{s,j}-U_{g,j})}{\tau_{st}}+\epsilon_s\frac{\partial p_g}{\partial x_j}-\epsilon_s\rho_sG_j,\\ &<\frac{u_j^2}{2}\mathcal{A}_i>=\frac{\epsilon_s\rho_sU_{s,j}(U_{s,j}-U_{g,j})}{\tau_{st}}+\frac{3p_s}{\tau_{st}}+\epsilon_sU_{s,j}\frac{\partial p_g}{\partial x_j}-\epsilon_s\rho_sU_{s,j}G_j,\\ &<\xi^2\mathcal{A}_i>=0.\end{aligned}$$

When $\psi_1=1$, Eq. (A.2) becomes

$$\frac{\partial<1>}{\partial t}+\frac{\partial<u_i>}{\partial x_i}+<\mathcal{A}_i>=0,$$

which leads to the mass conservation equation,

$$\frac{\partial(\epsilon_s\rho_s)}{\partial t}+\frac{\partial(\epsilon_s\rho_sU_i)}{\partial x_i}=0.$$

For ψ_α, $\alpha=2,3,4$, with $j=\alpha-1$ and $\psi_j=u_j$, Eq. (A.2) go to,

$$\frac{\partial<u_j>}{\partial t}+\frac{\partial<u_ju_i>}{\partial x_i}+<u_j\mathcal{A}_i>=0,$$

which are the momentum equations,

$$\frac{\partial(\epsilon_s\rho_sU_j)}{\partial t}+\frac{\partial(\epsilon_s\rho_sU_jU_i+p_s\delta_{ji})}{\partial x_i}+\frac{\epsilon_s\rho_s(U_{s,j}-U_{g,j})}{\tau_{st}}+\epsilon_s\frac{\partial p_g}{\partial x_j}-\epsilon_s\rho_sG_j=0.$$

Finally, taking $\psi_5=\frac{u_j^2+\xi^2}{2}$, Eq. (A.2) comes to

$$\frac{\partial<\frac{u_j^2+\xi^2}{2}>}{\partial t}+\frac{\partial<\frac{u_j^2+\xi^2}{2}u_i>}{\partial x_i}+<\frac{u_j^2+\xi^2}{2}\mathcal{A}_i>=0,$$

which corresponds to the energy equation,

$$\frac{\partial(\epsilon_s\rho_s E_s)}{\partial t}+\frac{\partial(\epsilon_s\rho_s E_s U_{s,i}+p_s U_{s,i})}{\partial x_i}+\frac{\epsilon_s\rho_s U_{s,j}(U_{s,j}-U_{g,j})}{\tau_{st}}+\frac{3p_s}{\tau_{st}}+\epsilon_s U_{s,j}\frac{\partial p_g}{\partial x_j}-\epsilon_s\rho_s U_{s,j}G_j=0,$$

where $\epsilon_s\rho_s E_s=\frac{1}{2}\epsilon_s\rho_s U_{s,j}^2+\frac{K_s+3}{2}p_s$.

References

[1] Michael J Andrews and Peter J O'Rourke. The multiphase particle-in-cell (MP-PIC) method for dense particulate flows. *International Journal of Multiphase Flow*, 22(2):379–402, 1996.

[2] MR Baer and JW Nunziato. A two-phase mixture theory for the deflagration-to-detonation transition (DDT) in reactive granular materials. *International Journal of Multiphase Flow*, 12(6):861–889, 1986.

[3] S Balachandar and John K Eaton. Turbulent dispersed multiphase flow. *Annual Review of Fluid Mechanics*, 42:111–133, 2010.

[4] Prabhu Lal Bhatnagar, Eugene P Gross, and Max Krook. A model for collision processes in gases I: Small amplitude processes in charged and neutral one-component systems. *Physical Review*, 94(3):511–525, 1954.

[5] Graeme Austin Bird. Molecular gas dynamics. *NASA STI/Recon Technical Report A*, 76:40225, 1976.

[6] Guiyu Cao, Liang Pan, and Kun Xu. Three dimensional high-order gas-kinetic scheme for supersonic isotropic turbulence I: Criterion for direct numerical simulation. *Computers & Fluids*, 192(104273), 2019.

[7] Guiyu Cao, Hongmin Su, Jinxiu Xu, and Kun Xu. Implicit high-order gas kinetic scheme for turbulence simulation. *Aerospace Science and Technology*, 92:958–971, 2019.

[8] Sydney Chapman and Thomas George Cowling. *The Mathematical Theory of Non-Uniform Gases: An Account of the Kinetic Theory of Viscosity, Thermal Conduction and Diffusion in Gases*. Cambridge University Press, 1970.

[9] Yipei Chen, Yajun Zhu, and Kun Xu. A three-dimensional unified gas-kinetic wave-particle solver for flow computation in all regimes. *Physics of Fluids*, 32(9):096108, 2020.

[10] Alina Chertock, Shumo Cui, and Alexander Kurganov. Hybrid finite-volume-particle method for dusty gas flows. *The SMAI Journal of Computational Mathematics*, 3:139–180, 2017.

[11] Clayton T Crowe, John D Schwarzkopf, Martin Sommerfeld, and Yutaka Tsuji. *Multiphase Flows with Droplets and Particles*. CRC Press, 2011.

[12] Stephane De Chaisemartin, Frédérique Laurent, Marc Massot, and Julien Reveillon. Evaluation of Eulerian multi-fluid versus Lagrangian methods for ejection of polydisperse evaporating sprays by vortices. 2007.

[13] Olivier Desjardins, Rodney O Fox, and Philippe Villedieu. A quadrature-based moment method for dilute fluid-particle flows. *Journal of Computational Physics*, 227(4):2514–2539, 2008.

[14] Jianmin Ding and Dimitri Gidaspow. A bubbling fluidization model using kinetic theory of granular flow. *AIChE Journal*, 36(4):523–538, 1990.
[15] Rodney O Fox. A quadrature-based third-order moment method for dilute gas-particle flows. *Journal of Computational Physics*, 227(12):6313–6350, 2008.
[16] L Fréret, F Laurent, S de Chaisemartin, D Kah, RO Fox, P Vedula, J Reveillon, O Thomine, and M Massot. Turbulent combustion of polydisperse evaporating sprays with droplet crossing: Eulerian modeling of collisions at finite Knudsen and validation. In *Proceedings of the Summer Program*, pages 277–288. Citeseer, 2008.
[17] Nikolaj A Fuks. The mechanics of aerosols. Technical report, Chemical Warfare Labs Army Chemical Center MD, 1955.
[18] Wei Ge, Limin Wang, Ji Xu, Feiguo Chen, Guangzheng Zhou, Liqiang Lu, Qi Chang, and Jinghai Li. Discrete simulation of granular and particle-fluid flows: From fundamental study to engineering application. *Reviews in Chemical Engineering*, 33(6):551–623, 2017.
[19] Yu Guo and Jennifer Sinclair Curtis. Discrete element method simulations for complex granular flows. *Annual Review of Fluid Mechanics*, 47:21–46, 2015.
[20] Kee Soo Han and Myung Kyoon Chung. Numerical simulation of a two-phase gas-particle jet in a crossflow. *Aerosol Science and Technology*, 17(2):59–68, 1992.
[21] James E Hilton and Paul W Cleary. Comparison of non-cohesive resolved and coarse grain DEM models for gas flow through particle beds. *Applied Mathematical Modelling*, 38(17-18):4197–4214, 2014.
[22] Ryan W Houim and Elaine S Oran. A multiphase model for compressible granular-gaseous flows: Formulation and initial tests. *Journal of Fluid Mechanics*, 789:166, 2016.
[23] James T Jenkins, Stuart B Savage, et al. Theory for the rapid flow of identical, smooth, nearly elastic, spherical particles. *Journal of Fluid Mechanics*, 130(1):187–202, 1983.
[24] Xing Ji, Liang Pan, Wei Shyy, and Kun Xu. A compact fourth-order gas-kinetic scheme for the Euler and Navier-Stokes equations. *Journal of Computational Physics*, 372:446 – 472, 2018.
[25] Xing Ji, Fengxiang Zhao, Wei Shyy, and Kun Xu. A HWENO reconstruction based high-order compact gas-kinetic scheme on unstructured mesh. *Journal of Computational Physics*, 109367, 2020.
[26] RT Lahey Jr, M Lopez De Bertodano, and OC Jones Jr. Phase distribution in complex geometry conduits. *Nuclear Engineering and Design*, 141(1-2):177–201, 1993.
[27] Qibing Li, Song Fu, and Kun Xu. Application of gas-kinetic scheme with kinetic boundary conditions in hypersonic flow. *AIAA Journal*, 43(10):2170–2176, 2005.
[28] Weiming Li, Chang Liu, Yajun Zhu, Jiwei Zhang, and Kun Xu. Unified gas-kinetic wave-particle methods III: Multiscale photon transport. *Journal of Computational Physics*, 408:109280, 2020.
[29] Chang Liu, Zhao Wang, and Kun Xu. A unified gas-kinetic scheme for continuum and rarefied flows VI: Dilute disperse gas-particle multiphase system. *Journal of Computational Physics*, 386:264–295, 2019.
[30] Chang Liu and Kun Xu. A unified gas kinetic scheme for continuum and rarefied flows V: Multiscale and multi-component plasma transport. *Communications in Computational Physics*, 22(5):1175–1223, 2017.
[31] Chang Liu and Kun Xu. A unified gas-kinetic scheme for micro flow simulation based on linearized kinetic equation. *Advances in Aerodynamics*, 2(1):1–22, 2020.
[32] Chang Liu and Kun Xu. Unified gas-kinetic wave-particle method IV: Multi-species gas mixture and plasma transport. *Advances in Aerodynamics*, 3:9, 2021.
[33] Chang Liu, Yajun Zhu, and Kun Xu. Unified gas-kinetic wave-particle methods I: Contin-

uum and rarefied gas flow. *Journal of Computational Physics*, 401:108977, 2020.
[34] Xiaowen Liu, Limin Wang, and Wei Ge. Meso-scale statistical properties of gas-solid flow–a direct numerical simulation (DNS) study. *AIChE Journal*, 63(1):3–14, 2017.
[35] Liqiang Lu, Xiaowen Liu, Tingwen Li, Limin Wang, Wei Ge, and Sofiane Benyahia. Assessing the capability of continuum and discrete particle methods to simulate gas-solids flow using DNS predictions as a benchmark. *Powder Technology*, 321:301–309, 2017.
[36] Liqiang Lu, Aaron Morris, Tingwen Li, and Sofiane Benyahia. Extension of a coarse grained particle method to simulate heat transfer in fluidized beds. *International Journal of Heat and Mass Transfer*, 111:723–735, 2017.
[37] Liqiang Lu, Ji Xu, Wei Ge, Guoxian Gao, Yong Jiang, Mingcan Zhao, Xinhua Liu, and Jinghai Li. Computer virtual experiment on fluidized beds using a coarse-grained discrete particle method-EMMS-DPM. *Chemical Engineering Science*, 155:314–337, 2016.
[38] CKK Lun, S Br Savage, DJ Jeffrey, and N Chepurniy. Kinetic theories for granular flow: Inelastic particles in couette flow and slightly inelastic particles in a general flowfield. *Journal of Fluid Mechanics*, 140:223–256, 1984.
[39] Kun Luo, Zhuo Wang, Junhua Tan, and Jianren Fan. An improved direct-forcing immersed boundary method with inward retraction of Lagrangian points for simulation of particle-laden flows. *Journal of Computational Physics*, 376:210–227, 2019.
[40] Daniele L Marchisio and Rodney O Fox. *Computational Models for Polydisperse Particulate and Multiphase Systems*. Cambridge University Press, 2013.
[41] Florianr Menter. Zonal two equation k-ω turbulence models for aerodynamic flows. In *23rd Fluid Dynamics, Plasmadynamics, and Lasers Conference*, page 2906, 1993.
[42] Peter J O'Rourke and Dale M Snider. Inclusion of collisional return-to-isotropy in the MP-PIC method. *Chemical Engineering Science*, 80:39–54, 2012.
[43] Liang Pan, Junxia Cheng, Shuanghu Wang, and Kun Xu. A two-stage fourth-order gas-kinetic scheme for compressible multicomponent flows. *Communications in Computational Physics*, 22(4):1123–1149, 2017.
[44] Jooyeon Park and Hyungmin Park. Particle dispersion induced by vortical interactions in a particle-laden upward jet with a partial crossflow. *Journal of Fluid Mechanics*, 915, 2021.
[45] A Passalacqua, RO Fox, R Garg, and S Subramaniam. A fully coupled quadrature-based moment method for dilute to moderately dilute fluid-particle flows. *Chemical Engineering Science*, 65(7):2267–2283, 2010.
[46] Marica Pelanti and Randall J LeVeque. High-resolution finite volume methods for dusty gas jets and plumes. *SIAM Journal on Scientific Computing*, 28(4):1335–1360, 2006.
[47] Stefan Radl, Begona C Gonzales, Christoph Goniva, and Stefan Pirker. State of the art in mapping schemes for dilute and dense Euler-Lagrange simulations. 2015.
[48] X Rogue, G Rodriguez, JF Haas, and R Saurel. Experimental and numerical investigation of the shock-induced fluidization of a particles bed. *Shock Waves*, 8(1):29–45, 1998.
[49] T Saito. Numerical analysis of dusty-gas flows. *Journal of Computational Physics*, 176(1):129–144, 2002.
[50] Richard Saurel and Rémi Abgrall. A multiphase Godunov method for compressible multifluid and multiphase flows. *Journal of Computational Physics*, 150(2):425–467, 1999.
[51] Dale M Snider. An incompressible three-dimensional multiphase particle-in-cell model for dense particle flows. *Journal of Computational Physics*, 170(2):523–549, 2001.
[52] Wenjun Sun, Song Jiang, and Kun Xu. An asymptotic preserving unified gas kinetic scheme for gray radiative transfer equations. *Journal of Computational Physics*, 285:265–279, 2015.
[53] Shi Tao, Haolong Zhang, Zhaoli Guo, and Lian-Ping Wang. A combined immersed bound-

ary and discrete unified gas kinetic scheme for particle-fluid flows. *Journal of Computational Physics*, 375:498–518, 2018.

[54] Baolin Tian, Junsheng Zeng, Baoqing Meng, Qian Chen, Xiaohu Guo, and Kun Xue. Compressible multiphase particle-in-cell method (CMP-PIC) for full pattern flows of gas-particle system. *Journal of Computational Physics*, 418:109602, 2020.

[55] Zhao Wang and Hong Yan. Unified gas-kinetic scheme for the monodisperse gas-particle flow and its application in the shock-driven multiphase instability. *International Journal of Multiphase Flow*, 119:95–107, 2019.

[56] Zhao Wang and Hong Yan. Unified gas-kinetic particle method for dilute granular flow and its application in a solid jet. *Acta Mechanica Sinica*, 36(1):22–34, 2020.

[57] Kun Xu. BGK-based scheme for multicomponent flow calculations. *Journal of Computational Physics*, 134(1):122–133, 1997.

[58] Kun Xu. Gas-kinetic schemes for unsteady compressible flow simulations. *Lecture Series–van Kareman Institute for Fluid Dynamics*, 3:C1–C202, 1998.

[59] Kun Xu. A gas-kinetic BGK scheme for the Navier–Stokes equations and its connection with artificial dissipation and Godunov method. *Journal of Computational Physics*, 171(1):289–335, 2001.

[60] Kun Xu. A unified computational fluid dynamics framework from rarefied to continuum regimes. *Cambridge Elements Aerospace Enginnering*, 2021.

[61] Kun Xu and Juan-Chen Huang. A unified gas-kinetic scheme for continuum and rarefied flows. *Journal of Computational Physics*, 229(20):7747–7764, 2010.

[62] Xiaocong Xu, Yipei Chen, Chang Liu, Zhihui Li, and Kun Xu. Unified gas-kinetic wave-particle methods V: Diatomic molecular flow. *Journal of Computational Physics*, 442:110496, 2021.

[63] Xiaocong Xu, Yipei Chen, and Kun Xu. Modeling and computation for non-equilibrium gas dynamics: Beyond single relaxation time kinetic models. *Physics of Fluids*, 33(1):011703, 2021.

[64] Xiaojian Yang, Xing Ji, Wei Shyy, and Kun Xu. Comparison of the performance of high-order schemes based on the gas-kinetic and HLLC fluxes. *Journal of Computational Physics*, 448:110706, 2022.

[65] Liang Yu, Jing Lu, Xiangping Zhang, and Suojiang Zhang. Numerical simulation of the bubbling fluidized bed coal gasification by the kinetic theory of granular flow (KTGF). *Fuel*, 86(5-6):722–734, 2007.

[66] Fengxiang Zhao, Xing Ji, Wei Shyy, and Kun Xu. An acoustic and shock wave capturing compact high-order gas-kinetic scheme with spectral-like resolution. *International Journal of Computational Fluid Dynamics*, 2019.

[67] Fengxiang Zhao, Xing Ji, Wei Shyy, and Kun Xu. Compact higher-order gas-kinetic schemes with spectral-like resolution for compressible flow simulations. *Advances in Aerodynamics*, 1(1):13, 2019.

[68] Yajun Zhu, Chang Liu, Chengwen Zhong, and Kun Xu. Unified gas-kinetic wave-particle methods. II. Multiscale simulation on unstructured mesh. *Physics of Fluids*, 31(6):067105, 2019.

[69] Yajun Zhu and Kun Xu. The first decade of unified gas kinetic scheme. *arXiv preprint arXiv:2102.01261*, 2021.